Quaternary Research (2026), **129**, 19–35
doi:10.1017/qua.2025.10020

Research Article

Late glacial and Holocene climate and landscape dynamics in the Valdai Highlands (East European Plain) inferred from lake sediment records

Grigory Fedorov[a,b], Larisa Savelieva[c], Nikita Bobrov[c], Anna Ludikova[d], Natalia Kostromina[c], Anna Cherezova[c,e], Aleksey Petrov[c], Evgenia Bazhenova[c] and Andrei Andreev[f]

[a]Takhtajan Institute of Botany, National Academy of Sciences of the Republic of Armenia, Yerevan 0063, Armenia; [b]Arctic and Antarctic Research Institute, St. Petersburg 199397, Russia; [c]St. Petersburg State University, St. Petersburg 199034, Russia; [d]Institute of Limnology, Russian Academy of Sciences, SPC RAS, St. Petersburg 196105, Russia; [e]A.P. Karpinsky Russian Geological Research Institute, St. Petersburg 199106, Russia and [f]Alfred Wegener Institute, Helmholtz Centre for Polar and Marine Research, Potsdam 14473, Germany

Abstract

The results of a ground-penetrating radar survey and multiproxy studies of the sediment cores collected from two lakes in the Valdai Highlands (East European Plain) provide new insights into the late glacial and Holocene environmental history of the region situated in the marginal zone of the last Scandinavian ice sheet. The cores were analyzed for organic carbon and nitrogen content, as well as for pollen and diatoms. The chronology of the cores is based on radiocarbon dates and pollen-based stratigraphy. The studied records document that vast dead ice masses and associated ice-dammed lakes existed in the Valdai Highlands area until ~14 cal ka BP. Open tundra-steppe communities dominated the study area during the Oldest Dryas, Bølling, and Older Dryas (between ca. 17 and 14 cal ka BP), but dwarf birch (*Betula nana*), shrub alder (*Alnus fruticosa*), and willow (*Salix*) were also common. Scots pine forest (*Pinus sylvestris*) became common for a short interval during the Bølling warming (ca. 14.9 and 14.4 cal ka BP). The appearance of spruce (*Picea*) forest in the landscape occurred in the beginning of the Allerød warming (~14 cal ka BP), but the open steppe-like plant communities remained common until the onset of the Holocene. The modern lake systems emerged at ~10 cal ka BP, marked by an onset of organic-type sedimentation and the appearance of modern-type forests. The Mid-Holocene (~8–4 cal ka BP) was the warmest time, as documented by the maximal distribution of temperate and broadleaved taxa in the region. The onset of agricultural land use and simultaneous trend of increasing lake trophic state and increasing paludification in the area is recorded at ~2.5 cal ka BP.

Keywords: Dead ice masses; Ground-penetrating radar; Diatoms; Pollen; Environmental history

Introduction

The paleoenvironmental history of northwestern Russia during the late glacial and the Holocene has been the focus of many studies, especially in recent years (e.g., Davydova et al., 1992, 2001; Arslanov et al., 1999, 2001; Wohlfarth et al., 1999, 2002, 2004, 2006, 2007; Subetto et al., 2002; Subetto, 2009; Novenko et al., 2009; Payne et al., 2016; Gromig et al., 2019; Savelieva et al., 2019; Tarasov et al., 2019). However, spatial and temporal patterns of environmental changes in many localities of this vast region during the glacial/interglacial transition remain poorly studied due to the limited number of the records with reliable geochronological and paleoenvironmental data.

The Valdai Highlands (Fig. 1) is one such area with a poorly studied paleoenvironmental late glacial and Holocene history. The region was in the ice-marginal zone of the Scandinavian Ice Sheet (SIS) during the last glacial maximum (LGM) and was deglaciated shortly after the LGM (Verbitskiy et al., 2012). According to recent reconstructions (Hughes et al., 2016; Gorlach et al., 2017), the area was released from the ice between 17.5 and 16 cal ka BP (Fig. 1); however, this could have happened earlier. For example, Gromig et al. (2019), based on varve studies of the Lake Ladoga sediments, estimate the minimum age of the Luga Moraine as 14.5 cal ka BP and the maximum as 15.9 cal ka BP. If these estimations are correct, the SIS ice margin at 16 cal ka BP should be located much farther to the north and northwest (Fig. 1). Large proglacial lakes presumably existed south of the SIS in the Valdai area (e.g., Gorlach et al., 2017 and references therein). According to Demidov et al. (2006), the SIS deglaciation in northwestern Russia was characterized by the long-lasting presence of dead ice masses. However, there are no data confirming the time of preservation and influence of dead ice masses on the landscape evolution of the Valdai Highlands.

Our study area is located on the northeastern slope of the Valdai Highlands (Fig. 1). According to Hughes et al. (2016), this is about 10–20 km north of the southern limit of the SIS in northwestern Russia during the LGM. Therefore, the detailed environmental history of this area will help provide a better understanding of the deglaciation of northwestern Russia. In this paper, we present the

Corresponding author: Andrei Andreev; Email: aandreev@awi.de
Cite this article: Fedorov, G., Savelieva, L., Bobrov, N., Ludikova, A., Kostromina, N., Cherezova, A., Petrov, A., Bazhenova, E., Andreev, A., 2026. Late glacial and Holocene climate and landscape dynamics in the Valdai Highlands (East European Plain) inferred from lake sediment records. *Quaternary Research* **129**, 19–35. https://doi.org/10.1017/qua.2025.10020

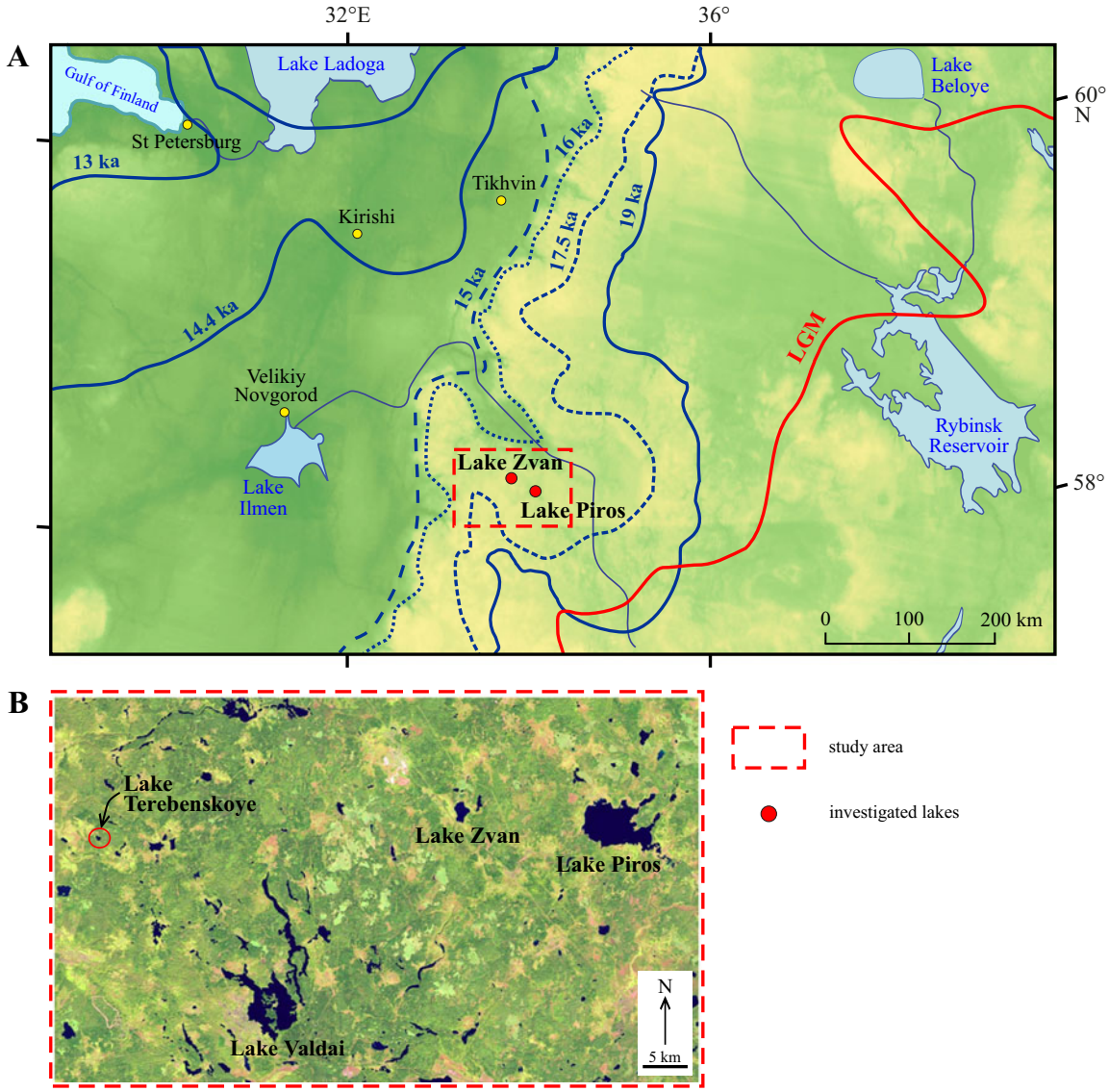

Figure 1. Location of the study area in northwestern Russia. (**A**) Topographic map indicating the location of the study area. (**B**) Satellite image showing the study area with locations of the investigated lakes and other lakes mentioned in the text. The most probable deglacial ice-margin positions (blue lines) are according to Hughes et al. (2016) and Gorlach et al. (2017). The maximal LGM ice-margin position (red line) is according to Hughes et al. (2016).

environmental history of the Valdai Highlands after deglaciation, basing the results on ground-penetrating radar (GPR) profiling of two lakes, analysis of lacustrine lithological facies, and on detailed multiproxy studies of lake sediment cores. The studies included measurements of total organic carbon (TOC) and nitrogen (TN), radiocarbon (^{14}C) dating of sediments, and pollen and diatom analyses.

Geographic and geological setting of the study area

The Valdai Highlands extend for approximately 600 km from the southern extremity of Lake Onega to the upper reaches of the Lovat River and consist of a series of separate ridges that shape the watershed between the Baltic and Caspian Seas. The maximum elevation of the Valdai Highlands is 346 m above sea level (m asl) (Verbitskiy et al., 2012). The area was marginal for the SIS because of its position within a huge positive pre-Quaternary landform, the so-called Carboniferous Plateau (Krotova-Putintseva and Verbitskiy, 2012; Verbitskiy et al., 2012; Kalm and Gorlach, 2014). In the north, this plateau is separated from the lowland by a ledge, with contours repeating the Valdai Highlands form.

The studied lakes are located in the northeast margin of the Valdai Highlands (Fig. 1). The modern Lake Piros (58°08′N, 33°53′E, 154 m asl) covers an area of ~31.5 km² with a maximum water depth of ~11.5 m and has a catchment of ~2120 km². It is drained through the Berezayka River into the Msta River, and farther through the Lake Ilmen and Lake Ladoga to the Baltic Sea.

The modern Lake Zvan (58°09′N, 33°37′E, 180.6 m asl; Fig. 2), situated about 12 km from Lake Piros, covers an area of ~15 km² with a maximum water depth of ~4.5 m and has a catchment of ~45 km². Previously, the lake drained through the Zvanka and Valdaika Rivers to Lake Piros, but in recent decades, it has turned into an enclosed basin, likely due to human activities that have resulted in eutrophication and paludification processes in the lake basin.

https://doi.org/10.1017/qua.2025.10020 Published online by Cambridge University Press

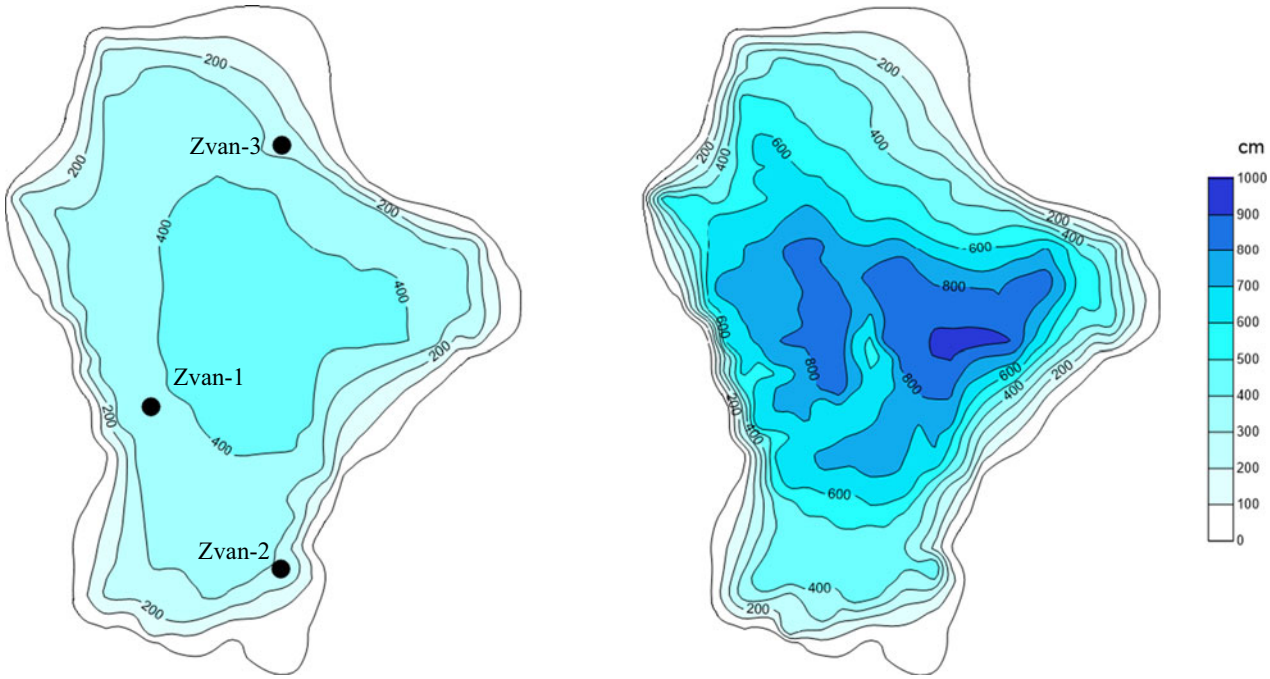

Figure 2. Maps of Lake Zvan plotted based on the ground-penetrating radar (GPR) profiling data. (**A**) Bathymetric map of Lake Zvan showing the coring sites. (**B**) Depth of the GPR Unit IV surface. Depths are in centimeters below the water level. Isolines are drawn at intervals of 100 cm.

The bedrock in the study area is Lower Carboniferous limestone, lying directly under the Quaternary deposits (Bushtuev et al., 1971). The main geomorphological features around the lakes were formed by glacial processes. However, the karst, which formed local landforms before the Quaternary, continues to play a substantial role in the modern geological processes (Bushtuev et al., 1971; Musin and Kirsanov, 1990). Numerous karst sinkholes, disappearing streams, and springs have been observed around the lakes (Musin and Kirsanov, 1990).

The modern climate of the area is boreal with mildly warm summers and prolonged winters. The average annual temperature ranges between 2.9°C and 4.3°C. Humidity is relatively high throughout the year. The average annual precipitation varies from 540 to 750 mm (Bushtuev et al., 1971). Mixed forests with spruce (*Picea*), birch (*Betula*), alder (*Alnus*), Scots pine (*Pinus sylvestris*), and some broadleaved species (oak (*Quercus*), lime (*Tilia*), elm (*Ulmus*)) dominate the vegetation in the southern part of the Valdai Highlands.

Material and methods

GPR profiling

To obtain a large-scale overview of the past depositional processes in the lake basins, GPR profiling was performed in both lakes during the summers of 2014 and 2015. The GPR survey was carried out from the board of an inflatable motorboat moving at a speed of ca. 4 km/h, using the "Oko" radar with a shielded antenna unit AB-150 (150 MHz), mounted on the bottom of another inflatable boat towed close to the motorboat. The total length of the GPR profiles is ~12 km for Lake Zvan and ca. 18 km for Lake Piros.

The measurements were carried out in a continuous mode with a constant time step between the radar traces, each therefore having a time reference. Simultaneously with the GPR profiling, a GPS track was logged, which also contains time stamps. Consequently, interpolating between the GPS track points allows one to determine the spatial coordinates of the recording points for each trace of the radargram. The data are plotted as grayscale radargrams. Minimal data processing was performed, which included correction of zero, adjustment of scale and signal amplification, and in some parts, band-pass filtering to remove noise and the very low frequency trend. Direct wave was not removed.

In the presented radargrams (GPR time sections), the horizontal axis corresponds to the distance along the profile measured in meters; the vertical axis is the time measured in nanoseconds. No depth scale is placed on the figures, as the depth of the reflecting surfaces cannot be directly calculated due to different velocities of GPR waves in water and sediments. The GPR wave velocity in silt was estimated for Lake Zvan in order to reconstruct the basement isosurface (Fig. 2). The lowermost reflecting boundary seen in the radargrams is assumed to be the basement.

Sediment coring and core handling

The coring of lake sediments was performed in February 2014 (core Zvan-1) and February 2015 (cores Zvan-2, Zvan-3, and Piros-1) from the ice with a Russian peat corer (1 m sampling part, 7 cm diameter). Detailed information for the core locations is presented in Table 1. The detailed lithological descriptions and detailed core photography were performed in the laboratories of the Arctic and Antarctic Research Institute and St. Petersburg State University before the cores were subsampled for analyses.

Pollen analysis

Pollen samples from the organic-rich lake sediments (gyttja) were prepared using the alkaline method (Grichuk and Zaklinskaya, 1948), while samples from the bottom sediments containing sand, silt, and clay were prepared using the heavy liquid separation

https://doi.org/10.1017/qua.2025.10020 Published online by Cambridge University Press

Table 1. Studied sediment cores from two lakes in the Valdai Highlands.

Core ID	Coordinates	Water depth (cm)	Core length (cm)
Zvan–1	58°09′40.0″N 33°37′17.6″E	416	424
Zvan–2	58°09′23.3″N 33°37′42.7″E	330	460
Zvan–3	58°10′06.5″N 33°37′43.5″E	308	69
Piros–1	58°09′49.5″N 33°53′38.5″E	472	494

method (Grichuk and Zaklinskaya, 1948). Additionally, all samples were sieved at 7 mm ultrasonic fine-sieving for 3 min (Cwynar et al., 1979). Water-free glycerol was used for sample storage and preparation of microscopic slides. Pollen and spores were identified by light microscope MIKMED-6 at 400× magnification with the aid of published pollen keys and atlases (Kupriyanova and Alyoshina, 1978; Moore et al., 1991) and the modern pollen reference collection of the St. Petersburg State University. At least 300 pollen grains of terrestrial plants were counted in the samples from the organic-rich sediments and 150 in the samples from the mineral-rich bottom sediments. Colonies of green algae (*Pediastrum* and *Botryococcus*) were also counted. The relative frequencies of pollen taxa were calculated from the sum of the terrestrial pollen taxa. The percentages of spore taxa are based on the sum of pollen and spores. The percentages of green algae remains are based on the sum of pollen and algae remains. TGView software (Grimm, 2004) was used to calculate percentages and draw the pollen diagrams. The diagrams were zoned by a qualitative inspection of notable changes in pollen assemblages and the occurrence of particular indicator taxa.

Diatom analysis

Samples were dried at 20°C and then weighed for further calculation of diatom concentrations. Dried samples were treated with 30% H_2O_2 to remove organic matter. A pretreatment with 10% HCl was performed for samples from the bottom (mineral-rich) part of the core, which contained sedimentary carbonates. Fraction separation in a heavy liquid (CdI_2 + KI, density of 2.6 g/cm^3) was applied only for the samples from mineral-rich sediments. After repeated washing in distilled water, the residual material was diluted with a measured amount of water and stirred carefully, before 0.1 mL of the decanted sample was placed on a cover glass, allowed to dry, and mounted on a slide using the synthetic resin Elyashev's medium (refractive index n = 1.67–1.68). At least 500–600 diatom valves were counted by light microscope MBI-15 at 1000× magnification in each sample, and 700–800 valves were counted in the samples with a dominance of small benthic Fragilariaceae in order to reveal underrepresented taxa. Diatom identification followed Krammer and Lange-Bertalot (1986, 1988, 1991a, 1991b), and the diatom taxonomy was subsequently updated according to AlgaeBase (Guiry and Guiry, 2024). Diatom ecological preferences are derived from Davydova (1985) and van Dam et al. (1994). Cysts of chrysophytes (golden algae, Chrysophyceae) were also counted. Absolute abundances (concentrations per 1 g of dry sediment) of diatom valves and chrysophyte cysts were calculated following Davydova (1985). The diatom diagram was built using the C2 v. 1.7 software (Juggins, 2007).

TOC and TN Content

TOC and TN were measured by a Vario EL III CHNS Elemental Analyzer (Elementar Ltd, UK). Freeze-dried sediment samples (60–70 mg) were ground to a fine powder and packed into tin and silver foil boats. The boats were weighed, closed tightly (to remove the air), and loaded into the sample carousel of the elemental analyzer. Nicotinamide ($C_6H_6N_2O$) and acetanilide (C_8H_9NO) were used as analytical standards. All measurements were repeated twice, and mean values were determined within a 95% confidence interval.

Chronostratigraphic methods

The ^{14}C dating was carried out by accelerator mass spectrometry (AMS) and conventional methods. The AMS ages were obtained in the Centre of Accelerator Mass Spectrometry (CologneAMS) at the University of Cologne, Germany, where bulk sediment samples and plant fragments were pretreated using the standard acid–alkali–acid extraction method to remove carbonates followed by sample combustion and conversion into elemental carbon (Rethemeyer et al., 2013). Conventional ^{14}C dating was performed at the Laboratory of Geomorphology and Palaeogeography of the Polar Regions and the World Ocean (St. Petersburg State University, Russia). All ^{14}C ages were calibrated using the IntCal20 calibration curve (Reimer et al., 2020).

Results

Sediment architecture and lithology

Four GPR stratigraphic units were identified in Lake Zvan (Fig. 3). The lower boundary of **Unit IV** is not recorded in the radargrams, and the sediments of this unit are intensively deformed. Some of the deformations are of a clearly sagging character (Fig. 3B, F, and G). The upper boundary of Unit IV has obvious traces of erosion. The Unit IV deposits are overlain discordantly by Unit III or Unit II (Fig. 3C and E). In the zones of non-deposition and wave erosion, the Unit IV deposits are exposed directly at the lake bottom (Fig. 3D). Figure 2 shows the contours of the modern lake bathymetry and the depth of the Unit IV surface calculated from the GPR results. A comparison of these bathymetric maps implies that lacustrine sedimentation leveled the initial complex lake-floor morphology, which comprised several small closed depressions, typical of karst and thermokarst processes.

Unit IV sediments are present only in the Zvan-1 and Zvan-3 cores (Figs. 3 and 4). In the Zvan-1 core, these sediments are detected between 315 and 424 cm. They can be interpreted as shallow-water sand sediments with some traces of wave erosion and, partly, as relatively deep-water silt and clay sediments with rhythmic lamination (Fig. 4A). In core Zvan-3, the Unit IV sediments are represented by sandy clays, overlain by coarse-grained gravelly sands (Fig. 4C).

The sediments of **Unit III** are present in the Zvan-1 and Zvan-2 cores (Figs. 3B and C and 4A and B). They are represented by two main sediment facies: relatively thin (ca. 60 cm) stratified silty layers within larger and deeper lake basins (Fig. 3E) and thicker (up to 420 cm) layers of massive sediments within small sediment pockets formed in ancient karst and/or thermokarst depressions (Fig. 3C). The Zvan-1 coring site is located within a larger basin, where the deposits of Unit III (Figs. 3B and 4A) are relatively thin and composed of silt with a high content of organic detritus. A horizon associated with wave action and slight erosion is observed

https://doi.org/10.1017/qua.2025.10020 Published online by Cambridge University Press

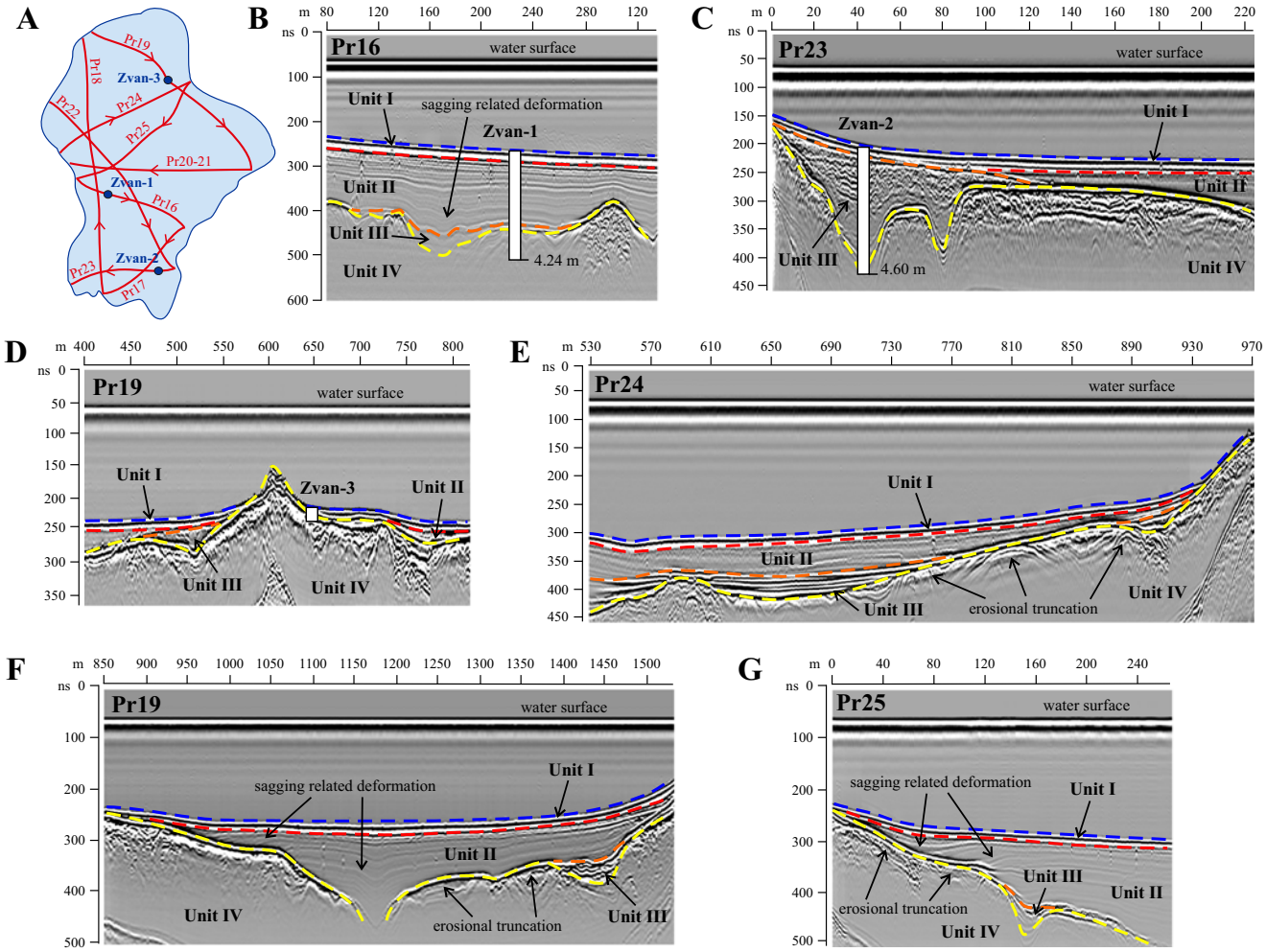

Figure 3. Fragments of the ground-penetrating radar (GPR) profiles obtained from Lake Zvan indicating coring positions, boundaries of the GPR stratigraphic units, and the main features of the sediment architecture. (**A**) Positions of the GPR profiles. (**B**) Fragment of profile Pr16 with the core Zvan-1 location. (**C**) Fragment of profile Pr23 with the core Zvan-2 location in the peat pocket. (**D**) Fragment of profile Pr19 with the core Zvan-3 location. (**E**) Fragment of profile Pr24 with a clear indication of erosional truncation between the GPR units IV and III and IV and II. (**F**) Fragment of profile Pr19 with clear indication of erosional truncation and sagging-related deformations. (**G**) Fragment of profile Pr25 with a closer view of the sagging-related slump.

at 311–306 cm depth (Fig. 4A). The Zvan-2 core was collected in a sediment pocket (Fig. 3C) with substantially thicker Unit III deposits (Figs. 3C and 4B). In the lower part of this core, they are represented by laminated silts with a high content of organic detritus pointing to accumulation in a lacustrine environment, while in the upper part, they are composed of peat, pointing to accumulation in a boggy environment.

Unit II deposits (stratified dark-brown unconsolidated gyttja) are present only in the Zvan-1 core (Fig. 4A). These sediments also demonstrate numerous traces of sagging-related deformations, but their degree is weaker than in the Unit IV deposits (Fig. 3). The thickness of the Unit II sediments in Lake Zvan depends on the depth of the initial lake subbasins (e.g., karst depressions) (Fig. 3).

Unit I deposits (stratified brown unconsolidated gyttja up to 50 cm thick) are present in the Zvan-1 and Zvan-2 cores (Figs. 3B and C and 4A and B).

The GPR profiling of Lake Piros has revealed a simpler lake stratigraphy (Fig. 5) than in Lake Zvan, probably because this lake is deeper. Nevertheless, the radargrams clearly reflect the older deformed deposits with complex surface geometry overlain by unconsolidated lacustrine sediments. The 494-cm-long sediment core (Piros-1) was retrieved from an ancient delta (prodelta) area (Fig. 5). A visible erosional contact at 394 cm core depth separates the sandy silt from the overlying gyttja (Fig. 6).

Chronology

To establish age–depth models for the studied cores, twelve ^{14}C ages were obtained from both lakes including seven by the AMS method and five by the conventional method (Table 2). The reliable dates have been used to construct Bayesian age–depth models for Zvan-1 and Piros-1 (Figs. 7 and 8). The Allerød and Younger Dryas oscillations, revealed in the Zvan-1 and Piros-1 pollen records (Figs. 9 and 10), were used as tie points in the construction of the models. We used age boundaries for the oscillations (12,737 ± 31 cal yr BP for Allerød/Younger Dryas boundary and 11,535 ± 58 cal yr BP for Younger Dryas/Holocene boundary) according to Lohne et al. (2013) and Mangerud (2021). The age–depth calculation was performed using the rBacon library (Blaauw and Christen 2011; Blaauw et al. 2020) for R (McKay et al. 2021).

https://doi.org/10.1017/qua.2025.10020 Published online by Cambridge University Press

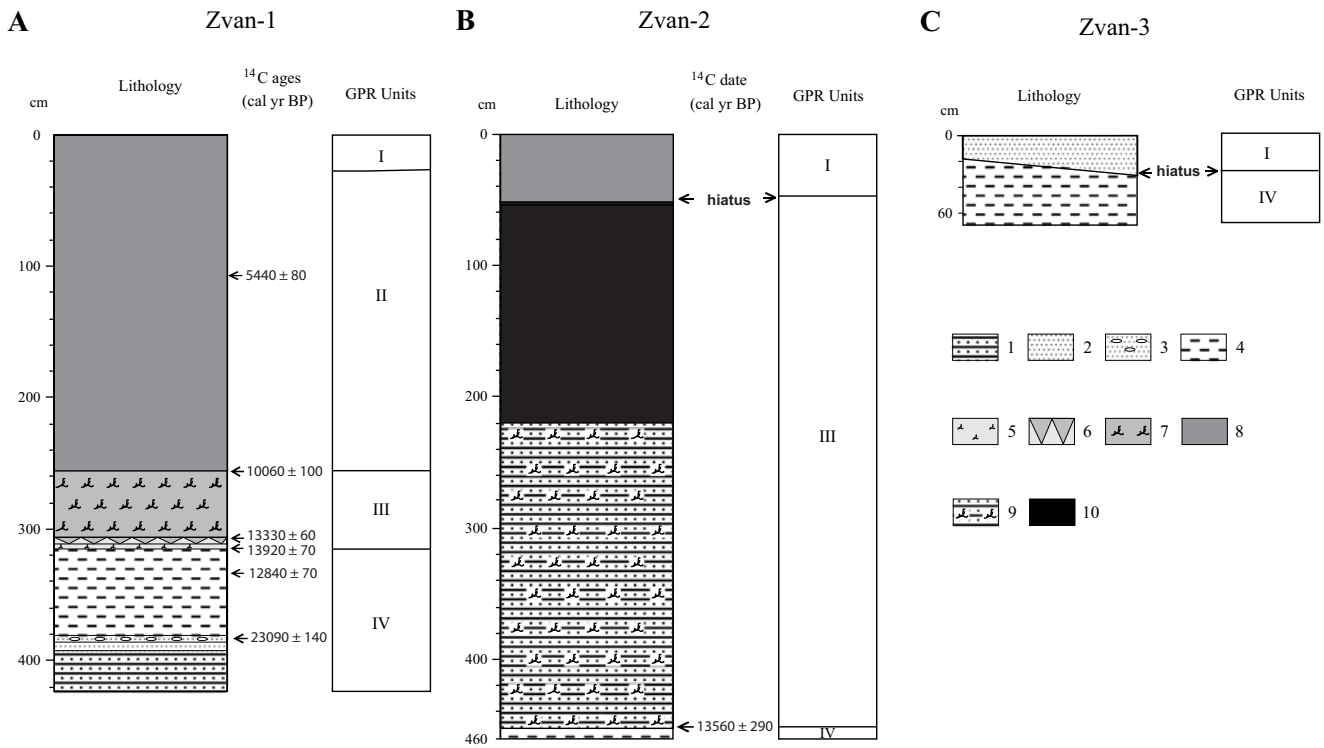

Figure 4. Lithology and stratigraphy of sediment cores collected in Lake Zvan. (**A**) Sediment core Zvan-1. (**B**) Sediment core Zvan-2. (**C**) Sediment core Zvan-3. 1, alternation of fine sand and silt; 2, fine sand; 3, fine sand with small pebbles; 4, planar-parallel rhythmically laminated clayey silt; 5, consolidated silt with low content of organic debris; 6, horizon associated with wave erosion; 7, laminated to consolidated silt with high content of organic debris; 8, consolidated detritus gyttja; 9, alternation of fine sand and silt with high content of organic debris; 10, peat.

Zvan-1 core chronology

Six ^{14}C dates have been obtained from the sedimentary sequence Zvan-1 (Table 2). Unfortunately, the dates from the lowest 65 cm are not reliable. The ^{14}C date 23,090 ± 140 cal yr BP from 382–381 cm core depth (Figs. 4A and 7; Table 2) corresponds to the so-called Middle Valdai mega-interstadial (Arslanov, 1993) and clearly contradicts the regional reconstructions of the LGM ice extent (Hughes et al., 2016; Gorlach et al., 2017; Rinterknecht et al., 2018). We suppose that the organic material was mostly redeposited from older sediments into the lake basin during the late glacial and reject this date from the age modeling. Another ^{14}C date, 12,840 ± 70 cal yr BP, from 332–331 cm core depth (Fig. 4A; Table 2), contradicts the pollen stratigraphy (Fig. 9), which clearly points to Allerød and Younger Dryas intervals (305–295 and 295–285 cm, correspondingly) above this date and with the two ^{14}C dates: 13,330 ± 60 and 13,920 ± 70 cal yr BP (Fig. 4A; Table 2) from the upper part of the core as well. Therefore, we also reject this date from the age modeling. For our age–depth model for the Zvan-1 core (Fig. 7), we adapted Allerød/Younger Dryas and Younger Dryas/Holocene boundaries by Lohne et al. (2013) and Mangerud (2021).

Piros-1 core chronology

Five ^{14}C dates ranging from 13,900 to 2000 cal yr BP (Figs. 6 and 8; Table 2) have been obtained from the sedimentary sequence Piros-1. A sharp lithological transition from sandy silt to organic-rich gyttja at 394 cm core depth (Fig. 6) accompanied by clear traces of erosion and abrupt changes in pollen assemblages (Fig. 10) points to a substantial hiatus in the sediment accumulation at the core location. Pollen-based regional stratigraphy (e.g., Khotinsky, 1987; Khotinsky and Klimanov, 1997; Arslanov et al., 1999; Tarasov et al., 2019 and references therein) and a ^{14}C date above the erosional boundary demarcate the hiatus between ca. 10,300 and 7000 cal ka BP. This hiatus and pollen-based Allerød/Younger Dryas and Younger Dryas/Holocene boundaries were also taken into consideration for the construction of the age–depth model for the Piros-1 core (Fig. 8).

Pollen stratigraphy

Sediment Core Zvan-1

A total of 49 samples from the sediment core Zvan-1 were analyzed for pollen, spores, and green algae (Fig. 9). All palynomorphs found were well preserved. Mineralized pre-Quaternary spores and pollen (up to 20%) were observed between 424 and 270 cm core depths. The revealed pollen assemblages were subdivided into 10 pollen zones (PZ) and are presented in Table 3.

Sediment Core Piros-1

A total of 59 samples from the sediment core Piros-1 were analyzed for pollen, spores, and green algae (*Pediastrum*). The revealed pollen assemblages were subdivided into nine PZs (Fig. 10) and are presented in Table 4.

Diatom stratigraphy

A total of 53 samples from the Zvan-1 core sediments were analyzed for diatoms and siliceous microfossils (Fig. 11). The revealed diatom assemblages were subdivided into five diatom zones (DZ) and are presented in Table 5. The upper 9 cm of the core was not studied for diatoms because of insufficient core sediments for all kinds of analyses.

https://doi.org/10.1017/qua.2025.10020 Published online by Cambridge University Press

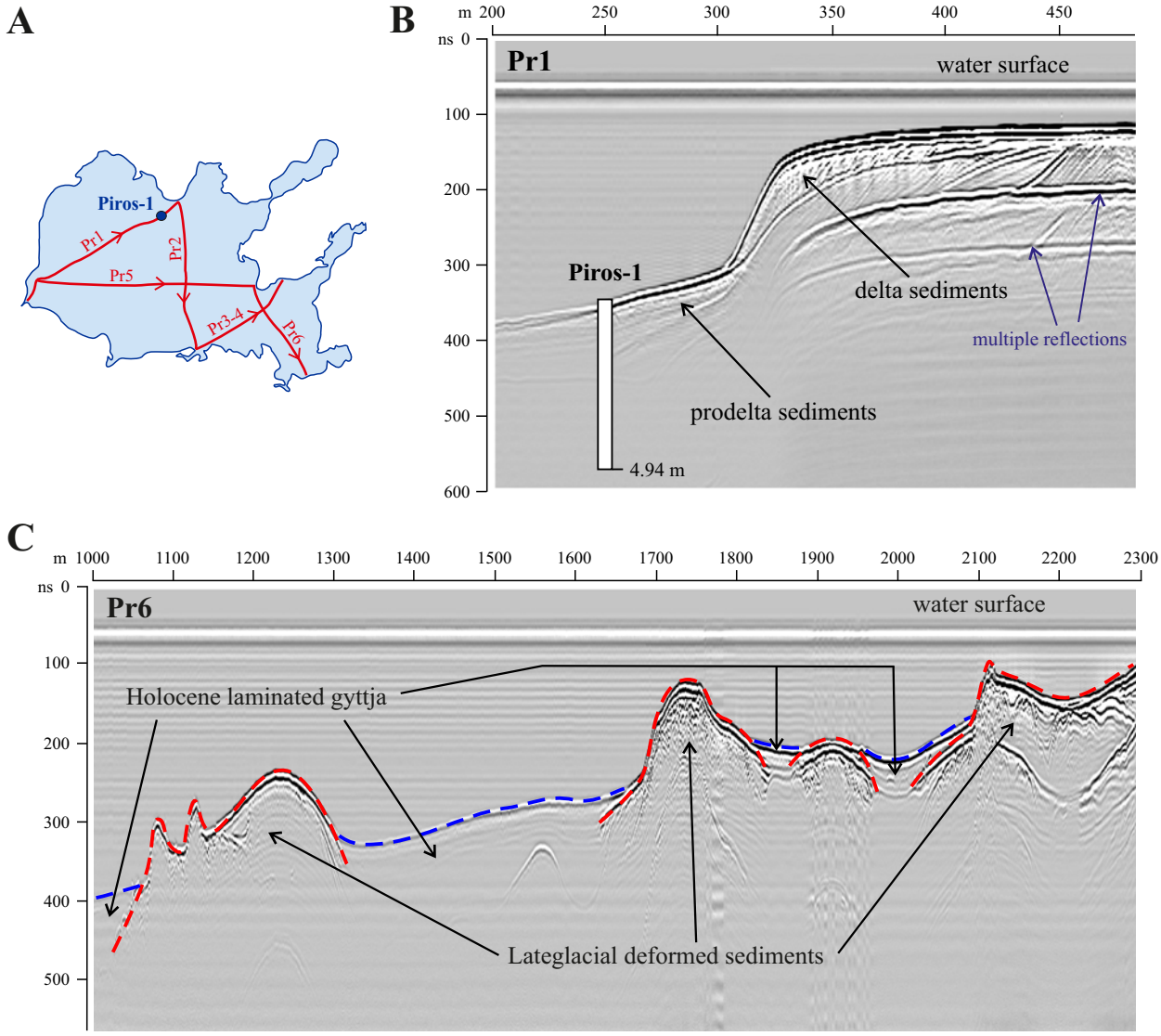

Figure 5. Fragments of the ground-penetrating radar (GPR) profiles obtained in Lake Piros showing the coring positions and the main features of the sediment architecture. (**A**) Positions of the GPR profiles. (**B**) Fragment of the profile Pr1 with the core Piros-1 location. (**C**) Fragment of the profile Pr6 with clear indication of an irregular contact between the older deformed deposits and overlying younger sediments.

TOC and TN content

Measurements of TOC and TN were carried out for the Zvan-1 sediment core (Fig. 7). In the lower part of the core (423–340 cm), TOC and TN are extremely low (0.5–0.6% and 0.05–0.1%, respectively). Large increases in both values are observed between 340 and 300 cm core depths (with TOC up to 7.7% and TN up to 0.8%), followed by a substantial decrease at 290 cm. Above 290 cm, the values further increase, reaching a maximum between 170 and 100 cm core depths (up to 24.3% for TOC and 2.2% for TN). The TOC:TN ratio shows a different trend (Fig. 7); although increasing gradually, it reaches a maximum (15.8) between 110 and 20 cm core depths.

Interpretations and discussion

Oldest Dryas

The oldest sediments were found in the Zvan-1 core. It is difficult to estimate the age of the bottom part because of a lack of reliable ^{14}C dates in the lower part of the core. However, taking into consideration the existing reconstructions of the SIS ice-marginal zone during the LGM (e.g., Hughes et al., 2016; Gorlach et al., 2017; Gromig et al., 2019 and references therein), we assume that the lacustrine accumulation in the initial lake basin started shortly after the deglaciation of the area, which may have occurred by 17 cal ka BP or even earlier. Thus, PZ I sediments (Fig. 9) were accumulated mostly during the Oldest Dryas, between the start of the deglaciation and 14.9 cal ka BP.

Pollen spectra document that open tundra-steppe communities with *Artemisia*, Cyperaceae, Poaceae, Chenopodiaceae (= Amaranthaceae), Asteraceae, and Rosaceae dominate in the study area. However, shrubs such as dwarf birches, alders, and willows were also common, indicating forest-tundra vegetation. Relatively high amounts of *Betula* sect. *Albae*, *Pinus*, and *Corylus* pollen might have a long-distant (wind-transported) origin, while very high amounts (up to 20%) of mineralized pre-Quaternary palynomorphs point to a reworked origin for these tree pollen taxa.

https://doi.org/10.1017/qua.2025.10020 Published online by Cambridge University Press

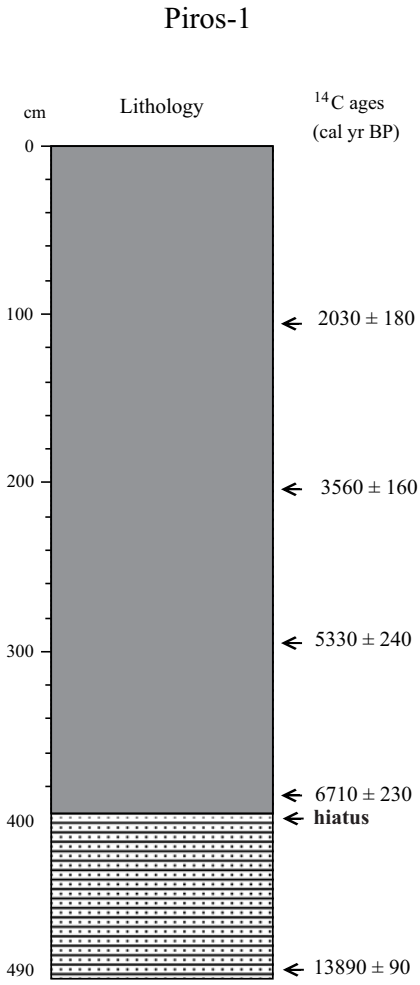

Figure 6. Lithology and stratigraphy of the sediment core Piros-1. The legend is shown in Figure 4 and defined in Figure 4 caption.

Table 2. ^{14}C dates from the studied sediment cores.

Core ID	Core depth (cm)	Dated material	^{14}C dates (yr BP)[a]	Calibrated ages (cal yr BP)	Lab. no.
Zvan−1	106−105	Bulk organic	4718 ± 37	5440 ± 80	COL2558.1.1
Zvan−1	255−254	Bulk organic	8940 ± 47	10,060 ± 100	COL2559.1.1
Zvan−1	305−304	Bulk organic	11,457 ± 49	13,330 ± 60	COL2560.1.1
Zvan−1	311−310	Plant remains	12,037 ± 54	13,920 ± 70	COL2561.1.1
Zvan−1	332−331	Plant remains	10,921 ± 55	12,840 ± 70	COL2563.1.1
Zvan−1	382−3812	Bulk organic	19,145 ± 93	23,090 ± 140	COL2564.1.1
Zvan−2	452−442	Bulk organic	11,640 ± 260*	13,560 ± 290	LU−8164
Piros−1	111−101	Bulk organic	2060 ± 140*	2030 ± 180	LU−8167
Piros−1	210−201	Bulk organic	3310 ± 130*	3560 ± 160	LU−8168
Piros−1	300−291	Bulk organic	4660 ± 190*	5330 ± 240	LU−8169
Piros−1	390−381	Bulk organic	5860 ± 200*	6710 ± 230	LU−8170
Piros−1	493−492	Bulk organic	11,983 ± 57	13,890 ± 90	COL3920.1.1

[a]Ages marked with asterisks (*) were obtained via the conventional ^{14}C method.

https://doi.org/10.1017/qua.2025.10020 Published online by Cambridge University Press

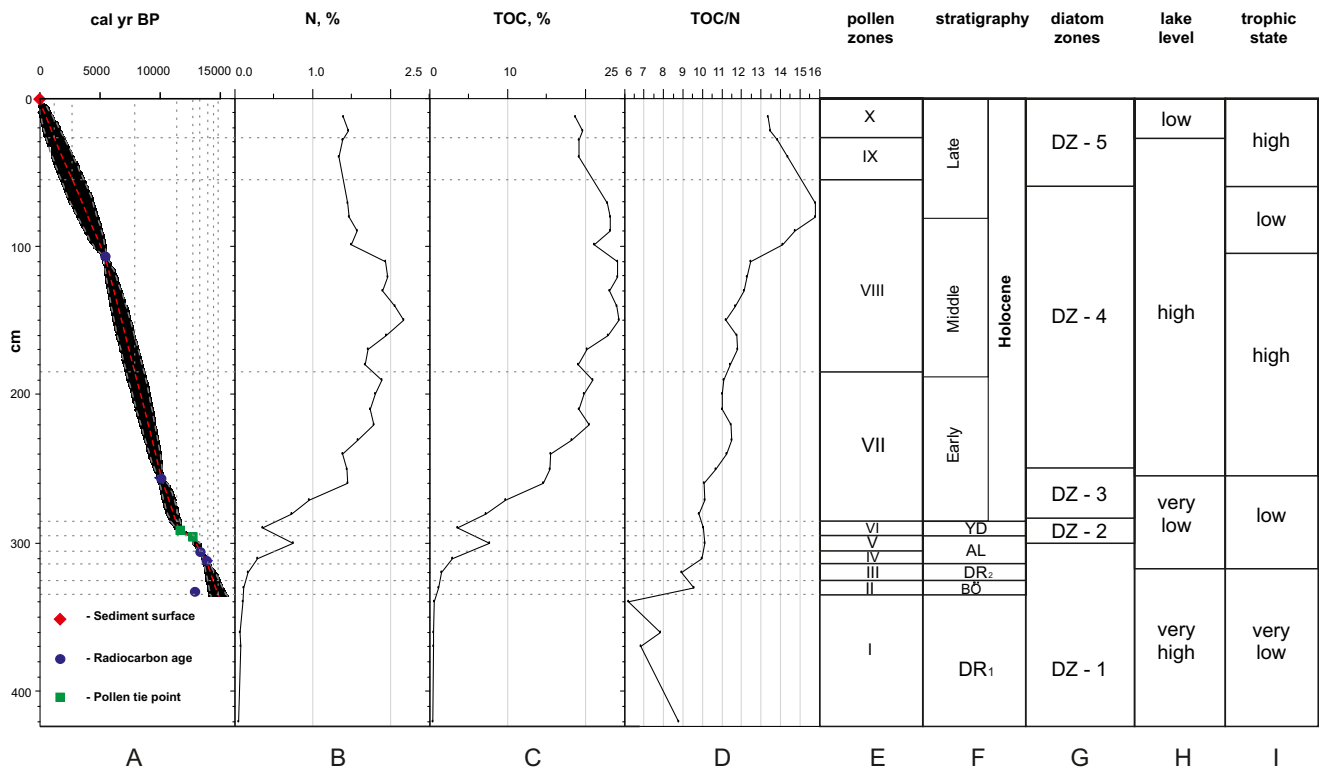

Figure 7. Sediment core Zvan-1 chronology, stratigraphy, organic geochemistry, and paleoenvironmental interpretation. (**A**) Age–depth model; (**B**) total nitrogen (TN); (**C**) total organic carbon (TOC) (**D**) TOC:TN ratio (TOC/N); (**E**) pollen zones; (**F**) stratigraphy; (**G**) diatom zones (DZ); (**H**) lake level; and (**I**) trophic state. YD, Younger Dryas; AL, Allerød; BO, Bølling; Dr_1, Oldest Dryas; Dr_2, Older Dryas.

Generally, the pollen assemblages (PZ I of Fig. 9) document harsh climatic conditions in the study area and correlate well with the Oldest Dryas records from northeastern Russia (e.g., Khotinsky, 1987; Khotinsky and Klimanov, 1997 and references therein).

The relatively numerous remains of green alga colonies (*Pediastrum* and *Botryococcus*) reflect the rather shallow-water habitats in the initial lake basin. The very low abundances of diatoms and cysts of chrysophytes in the sediments (Fig. 11) indicate active sedimentation processes in this initial basin lake.

Bølling

Contents of *Pinus* pollen substantially increase between ca. 14.9 and 14.4 cal ka BP (PZ II of Fig. 9), reflecting the possible presence of Scots pine in the lake catchment and warmer climate conditions during this interval. The revealed climate amelioration coincides well with the Bølling interstadial (ca. 14.7–14.1 cal ka BP). However, rather high percentages of herbs (especially *Artemisia* and Amaranthaceae) and a substantial decrease in the occurrence of shrubs point to relatively cool and dry climate conditions in the lake vicinity. Nevertheless, the disappearance of pre-Quaternary pollen and spores in the PZ II sediments suggest more stable soil conditions and denser vegetation cover in the lake catchment. The TOC and TN contents are slightly higher in the PZ II sediments compared with the extremely low contents in PZ I (Fig. 7). The increased C:N ratio (Fig. 7) indicates more allochthonous organic matter input, also pointing to warmer climate conditions. *Pediastrum* colonies are also substantially low in the PZ II sediments, which most likely reflects a higher lake level.

Older Dryas

PZ III pollen assemblages (Fig. 9) record the disappearance of Scots pine stands in the study area, which was covered mostly by open birch forests and steppe-like communities. This short-term cold stage can be correlated with the Older Dryas climate oscillation that occurred between the Bølling and Allerød interstadials about 14 ka BP. Its duration is not well defined; the estimates vary from 200 to 400 years. The increased amount of *Pediastrum* remains in the PZ III sediments points to numerous shallow-water habitats in the lake basin, presumably due to a lowering of water level in the lake at this time.

Allerød

A marked increase in *Picea* pollen percentages in the sediments is dated to ca. 13.9 cal ka BP (PZ IV of Fig. 9), documenting the appearance of spruce in the local vegetation and reflecting a substantial increase in summer temperatures and humidity. Percentages of *Picea* further increase in PZ V sediments (ca. 13.30–12.73 cal ka BP) and remain relatively high in the lower part of PZ VI until ca. 12.5 cal ka BP. The presence of spruce in the vegetation is associated with a continental climate with warm summers and moist soils (Giesecke and Bennett, 2004). The peak in *Picea* pollen percentages in the Zvan-1 core (ca. 13.30–12.73 cal ka BP) is simultaneous with the peaks in TOC and TN (Fig. 7), which also point to warmer climate conditions at this time. The bottom sediments of the Piros-1 core (PZ I of Fig. 10, ca. 14.0–12.1 cal ka BP) also have a high *Picea* pollen presence, suggesting the widespread distribution of spruce forests in the study area. The dominance of spruce in the local vegetation between ca. 14.0 and 12.5 cal ka BP)

https://doi.org/10.1017/qua.2025.10020 Published online by Cambridge University Press

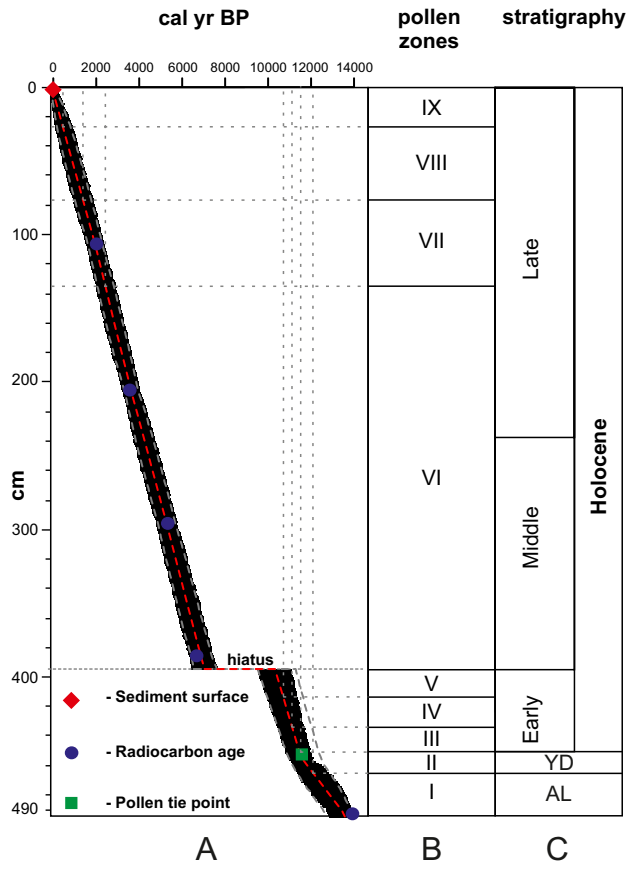

Figure 8. Sediment core Piros-1 chronology and stratigraphy. (**A**) Age–depth model; (**B**) pollen zones; and (**C**) stratigraphy. YD, Younger Dryas; AL, Allerød.

coincides well with the Allerød interstadial, which occurred from ca. 13.9–12.7 cal ka BP.

Generally, the marked increase of *Picea* pollen percentages in the Allerød sediments (the so-called lower peak of spruce), reflecting the appearance of spruce, has previously been reported in the central and northwestern parts of the East European platform (e.g., Khotinsky, 1987; Khotinsky and Klimanov, 1997; Kremenetski et al., 2000; Davydova et al., 2001; Latalowa and van der Knaap, 2006; Novenko et al., 2009; Savelieva et al., 2019; Tarasov et al., 2019 and references therein). However, the appearance of spruce in the Valdai Highlands was not properly dated. For example, Wohlfarth et al. (2007), based on the record from Lake Terebenskoye (approximately 40 km to the west of Lake Zvan; Fig. 1), suggest that the first appearance of spruce in the study area occurred only at 12 cal ka BP. From our pollen records (Figs. 9 and 10), the first appearance of spruce in the Valdai Highlands occurs around 14.0–13.9 cal ka BP, which is much earlier than previous estimations for the Valdai Highlands and ca. 600–800 years earlier than in the Lake Ladoga area (Savelieva et al., 2019).

Although spruce was a dominant forest taxon during the Allerød, birch was also a common tree in the local forests. High levels of herb pollen in the lake sediments suggest that open steppe- and tundra-like vegetation dominated by Poaceae, Cyperaceae, *Artemisia*, Amaranthaceae, Rosaceae, and *Thalictrum* was also broadly distributed in the area. Pre-Quaternary palynomorphs almost disappeared from the sediments, pointing to a substantial decrease in the erosional processes and denser vegetation cover. The increased C:N ratio also indicates more allochthonous organic matter input (Fig. 7). Colonies of the green alga *Pediastrum* significantly increase in the Allerød sediments compared with the Older Dryas sediments, reflecting the presence of numerous shallow-water habitats in the lake basin and warmer conditions.

Younger Dryas

A marked decrease in *Picea* pollen percentages in the Zvan-1 sediments (PZ VI of Fig. 9) after ca. 12.73 cal ka BP and around 12.6 cal ka BP in the Piros-1 sediments (PZ II of Fig. 10) reflect the disappearance of spruce from the local vegetation as a result of a substantial climate deterioration. Birch forests and open landscapes with dwarf shrubs, wormwoods, grasses, and sedges dominated the study area between ca. 12.7 and 11.5 cal ka BP. This cold and dry interval coincides well with the Younger Dryas stadial (Lohne et al., 2013; Mangerud, 2021).

Pollen percentages of tree birches and shrubs gradually increase in both sediment cores, while pollen of herbs (especially *Artemisia* and Amaranthaceae) decrease upward to the onset of the Holocene, reflecting a gradual climate amelioration (Figs. 9 and 10).

Early Holocene

The pollen assemblages in the sediments accumulated during the Early Holocene (PZ VII of Fig. 9 and PZ III and PZ V of Fig. 10) reflect a further development of the Scots pine and birch forests in the area, while typical late glacial communities dominated by *Artemisia*, Amaranthaceae, Rosaceae, and other herbs disappeared from the vegetation cover. Pre-Quaternary palynomorphs are almost absent in the Holocene sediments, reflecting that active erosion processes have stopped. More stable soil conditions and denser vegetation around the lakes resulted in a further increase in C and N content and the C:N ratio indicates more allochthonous organic matter input in the lake sediments (Fig. 7). The presence of aquatic pollen taxa (*Nuphar, Sparganium, Myriophyllum, Polygonum amphibium*, and *Typha*) in the Early Holocene sediments suggests more warm and stable aquatic environments in the lake. Thus, the Early Holocene pollen assemblages reflect the transition to the interglacial climatic conditions. Scots pine and birch were the dominant trees in the study area until ca. 8 cal ka BP. The first broadleaved taxa—elm and hazel (*Corylus*)—probably arrived in the Lake Zvan catchment by around 10.3 cal ka BP (PZ VII of Fig. 9). Elm is a thermophilic broadleaved tree species that began its expansion to the northwest Russian Plain after the last glaciation, when the temperature and moisture increased sufficiently to allow the northward migration of the thermophilic broadleaved trees from their southern refugia.

Mid-Holocene

During the Mid-Holocene (after 8 cal ka BP), alder and spruce, as well as thermophilic broadleaved trees including oak (*Quercus*), elm (*Ulmus*), hazel (*Corylus*), lime (*Tilia*), and ash (*Fraxinus*), became more common in the area, which was dominated by forests with spruce, Scots pine, birch, alder, and other broadleaved taxa. According to the pollen assemblages, the presence of the broadleaved taxa in the local vegetation was the highest between ca. 8 and 4 cal ka BP (PZ VIII of Fig. 9 and PZ VI of Fig. 10) reflecting the warmest climate conditions (Holocene thermal maximum) in the study area. Pollen of water caltrop (*Trapa natans*), a taxon especially indicative of relatively warm water conditions, was found in

https://doi.org/10.1017/qua.2025.10020 Published online by Cambridge University Press

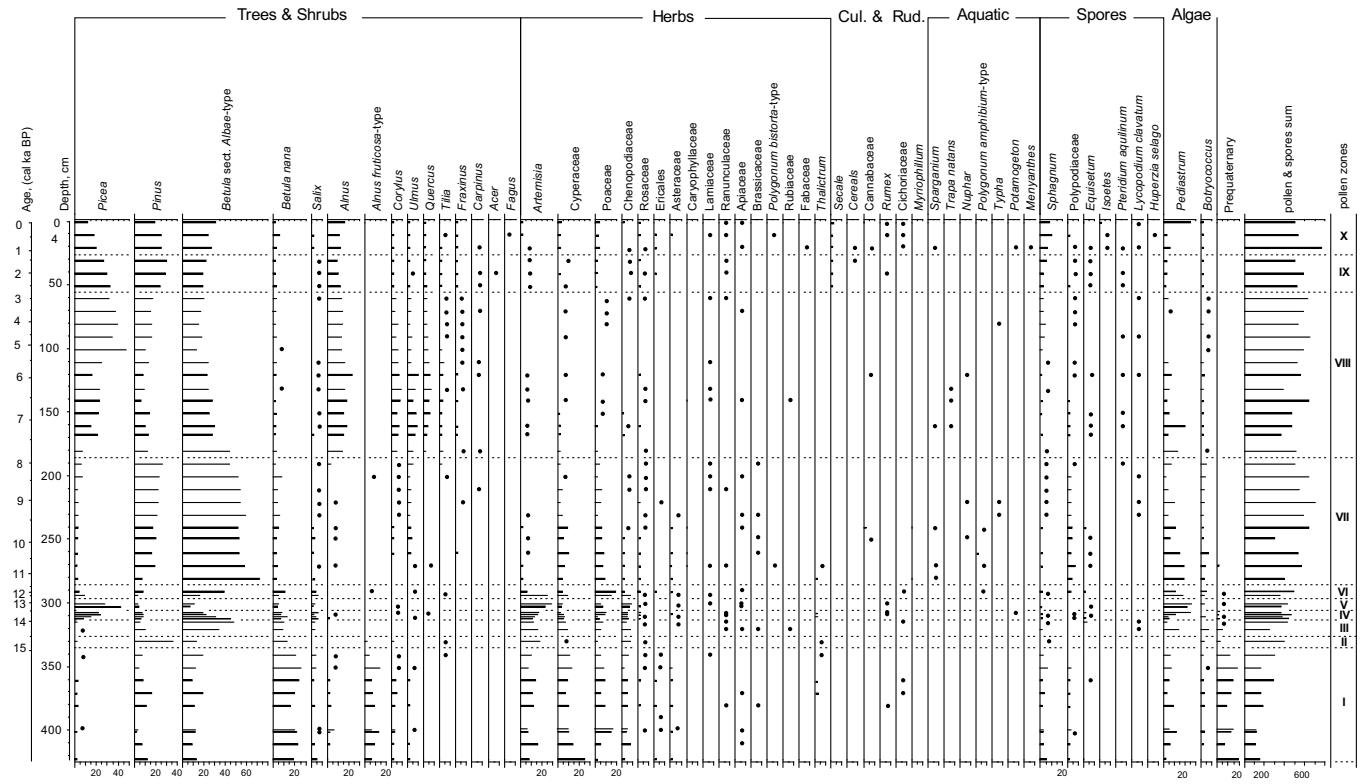

Figure 9. Percentage pollen diagram of the core Zvan-1. PZ, pollen zone.

Lake Zvan sediments (PZ VIII of Fig. 9), supporting the inference of the warmest climate during this time. TOC and TN reach their maximum values in the sediments accumulated during this time interval (Fig. 7), reflecting the highest bioproductivity in the lakes and thus confirming the warmest climate conditions during this Holocene thermal maximum. Low amounts of green alga colonies (*Pediastrum* and *Botryococcus*) in the Zvan sediments accumulated between ca. 8 and 4 cal ka BP (PZ VII of Fig. 9) probably reflect a higher lake level in Lake Zvan. The simultaneous slight increase in *Sphagnum* spore content may reflect the start of paludification in the lake's vicinity because of the higher lake level.

Late Holocene

Abundance of spruce and Scots pine in the local vegetation increased during the Late Holocene after 4 cal ka BP, while broadleaved taxa decreased. The study area was mostly dominated by spruce and mixed pine–birch–spruce forests with some broadleaved taxa. *Picea* pollen percentages reach their highest values in the Late Holocene sediments (PZ VIII of Fig. 9 and PZ VI of Fig. 10) and correlate well with the so-called upper maximum of spruce during the Subboreal period according to Khotinsky (1987). A further increase in *Sphagnum* spore content reflects wetter environments around Lake Zvan compared with the Middle and Early Holocene. These environmental changes point to a cooler and wetter climate in the study area.

The pollen assemblages from the sediments accumulated after ca. 2.5 cal ka BP (PZ IX and X of Fig. 9 and PZ VII–IX of Fig. 10) reflect local forests with spruce, Scots pine, birch, and alder dominating the study area. The pollen of cultivated cereals (rye (*Secale*) and probably wheat (*Triticum*)) were found in PZ IX (Fig. 9) and PZ VII (Fig. 10) dating from around 2.5 cal ka BP. We assume that they document the beginning of agricultural activity in the lakes' catchments. Generally, our new pollen records confirm previous evidence of agricultural land use in the Valdai region since ca. 2 cal ka (Novenko et al., 2009; Tarasov et al., 2019). However, it is not completely clear whether the agricultural activity in the catchments of Lake Zvan and Lake Piros started slightly earlier than in other parts of the Valdai Highlands and thus exemplifies differing rates of human colonization and migration processes in the different parts of the Valdai region, or whether it is just dating errors in previous studies and our lakes.

The upper PZs (PZ IX and X of Fig. 9 and PZ VII–IX of Fig. 10) also demonstrate a higher abundance of herb pollen such as grasses, sedges, and ruderals (e.g., *Rumex, Plantago, Urtica, Artemisia*, Asteraceae, Rosaceae), reflecting the active use of land around the lakes for the cultivation of crops and depasturing. The further decrease of broadleaved pollen taxa such as *Quercus* could also be a result not only of climate deterioration but also of human activity due to the selected use of trees.

The uppermost pollen spectra from the Piros-1 sediment core (PZ IX of Fig. 10) document some decrease in pollen of cultivated cereals and ruderals, which probably reflects a decline in agricultural activity during the last century.

Lake histories and landscape dynamics

Our study reveals that deposits of the GPR Unit IV (Fig. 4) in Lake Zvan were accumulated during the Oldest Drays, Bølling, and Older Drays, between ca. 17 and 14 cal ka BP. These deposits are well presented in the Zvan-1 core (Fig. 4A). Lithological features of the lower part of the core (424–381 cm core depth;

https://doi.org/10.1017/qua.2025.10020 Published online by Cambridge University Press

Table 3. Main pollen zones (PZ) of the Zvan-1 sediment core.

Pollen zones (cm)	Age (cal ka BP)	Dominant pollen assemblages
PZ I (424–335)	ca. 17.0–14.9	High content of non-arboreal pollen (NAP: up to 45%) represented mainly by *Artemisia* (up to 17%), Cyperaceae (25%), Poaceae (16%), Amaranthaceae (7%), Asteraceae (2%), and Rosaceae (2%). Pollen of *Betula nana* (20%) dominates the arboreal pollen (AP). The highest presence of pre-Quaternary microfossils (20%) and rather numerous remains of *Pediastrum* colonies are notable.
PZ II (335–325)	14.9–14.4	*Pinus* pollen increases up to 36%, while percentages of *Betula nana* and *Alnus fruticosa* significantly decrease.
PZ III (325–313)	14.4–13.0	High abundance of *Betula* sect. *Albae*–type pollen (up to 48%). *Artemisia* (15%) is the dominant NAP taxon. *Pediastrum* colonies increase to 20%.
PZ IV (313–305)	13.9–13.3	Significant increase in *Picea* pollen percentages (up to 25%) and high amounts of *Betula* sect. *Albae* (25%). *Artemisia* (16%), Amaranthaceae (5%), and Poaceae (5%) dominate NAP. High presence of *Pediastrum* (27%).
PZ V (305–295)	13.3–12.73	*Picea* pollen further increases, reaching 42%, while percentages of *Betula* sect. *Albae* decrease to 10%. *Artemisia* (28%), Amaranthaceae (7%), and Poaceae (6%) dominate NAP
PZ VI (295–285)	12.73–11.35	Marked decrease in *Picea* pollen percentages, while percentages of *Betula* sect. *Albae* pollen gradually increase to 38%, *Betula nana* to 13%, and *Salix* to 6%.
PZ VII (285–185)	11.35–7.90	*Betula* sect. *Albae* pollen percentages further increase (up to 70%). *Pinus* pollen percentages reach 22%. The appearance of *Ulmus* (up to 4%) and presence of aquatic pollen taxa (*Nuphar, Sparganium, Myriophyllum, Polygonum amphibium, Typha*) are also characteristic.
PZ VIII (185–55)	7.9–2.8	High abundance of *Picea* (up to 47%) and *Alnus* (22%) pollen. The abundance of broadleaved taxa (*Corylus, Ulmus, Quercus, Tilia*) are the highest for the whole record.
PZ IX (55–27)	2.80–1.25	High *Pinus* pollen percentages (up to 37%), while percentages of *Alnus, Corylus, Ulmus, Tilia,* and *Quercus* decrease. The pollen of cultured grasses (mostly *Secale*), and ruderal taxa appear. Poaceae pollen percentages also increase.
PZ X (27–0)	1.25–0	*Picea* and *Pinus* pollen percentages demonstrate a small decrease. while *Betula, Alnus*, Cyperaceae, Poaceae, and *Artemisia* increase. The pollen of *Secale* and other cereals are common. *Sphagnum* spores increase up to 12%.

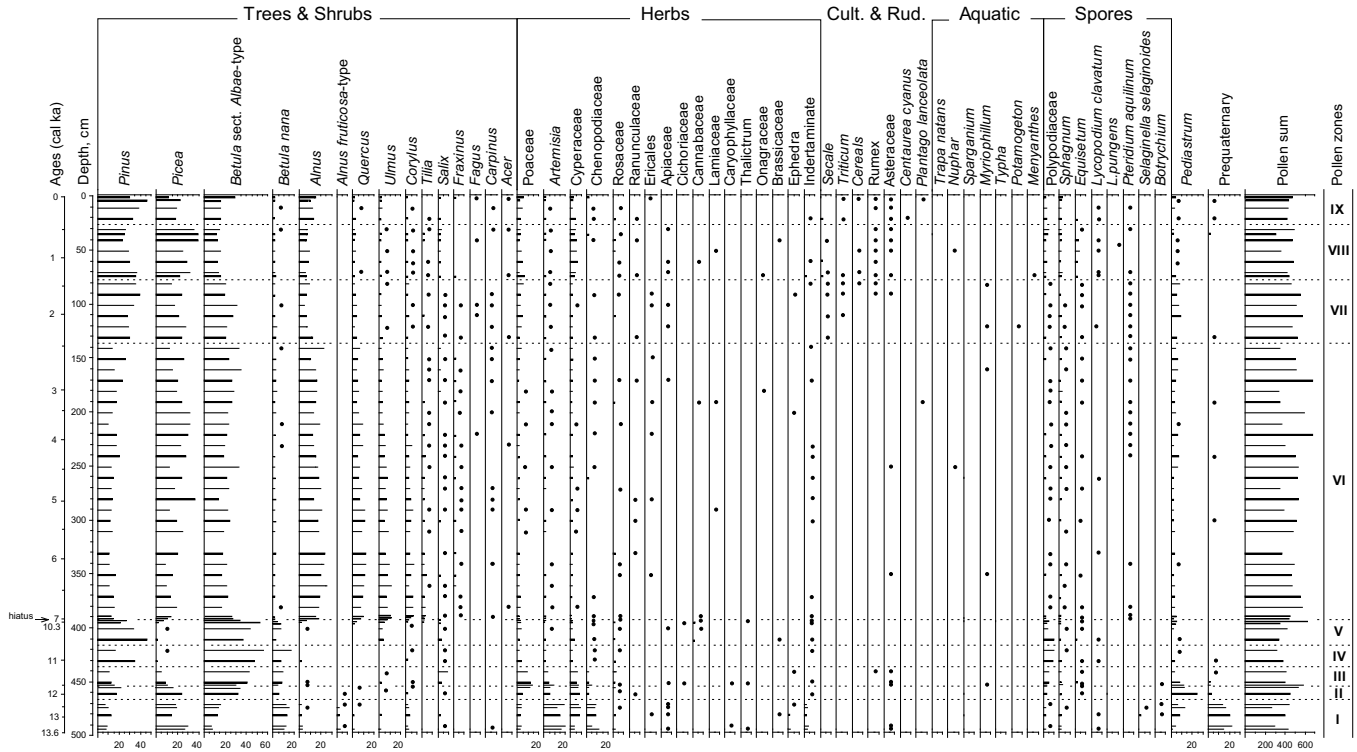

Figure 10. Percentage pollen diagram of the core Piros-1. PZ, pollen zone.

https://doi.org/10.1017/qua.2025.10020 Published online by Cambridge University Press

Table 4. Main pollen zones (PZ) of the Piros-1 sediment core.

PZ (cm)	Age (cal ka BP)	Dominant pollen assemblages
PZ I (494–465)	14.0–12.1	*Picea* (up to 30%), *Pinus* (20%), *Betula* sect. *Albae* (33%), *Betula nana* (15%), *Artemisia* (20%), Amaranthaceae (15%), and Cyperaceae 10% are dominant. Presence of *Ephedra* (2%) and high amounts of pre-Quaternary palynomorphs (22%) and *Pediastrum* (22%) are notable.
PZ II (465–453)	12.10–11.55	High percentages of *Betula* sect. *Albae* (up to 32%) and *Pinus* (18%) pollen are notable, while percentages of *B.* sect. *nana, Artemisia*, and Amaranthaceae significantly decrease. *Pediastrum* reaches 26%.
PZ III (453–435)	11.55–11.15	*Betula* sect. *Albae* pollen percentages increase up to 42%, while *Picea* is significantly reduced. The amount of *Pediastrum* is significantly reduced.
PZ IV (435–415)	11.15–10.75	Pollen of *Betula* sect. *Albae* (up to 56%), *Betula nana* (16%), and *Pinus* (20–35%) dominate.
PZ V (415–392)	10.75–7.00	Dominance of *Betula* sect. *Albae* (up to 50%) and *Pinus* (45%). Pollen of *Ulmus* appear in spectra (up to 2%).
PZ VI (392–135)	7.0–2.5	Significant increases of *Picea* (up to 34%), *Alnus* (25%), and *Ulmus* (10%).
PZ VII (135–77)	2.50–1.45	Abundance of broadleaved taxa and *Alnus* decrease, while *Picea* and Poaceae pollen slightly increase. *Secale* and *Triticum* pollen appear. Small increase in the amount of *Pediastrum*.
PZ VIII (77–25)	1.45–0.42	*Picea, Pinus, Betula* sect. *Albae*, and *Alnus* dominate. non-arboreal pollen (NAP) increases up to 15% (mostly Cyperaceae, Poaceae). The relatively high abundance of cultural cereals (mostly *Secale*), *Fagopyrum*, and ruderal (*Artemisia*, Amaranthaceae, *Rumex, Cannabis*) pollen taxa are notable. Further increase in the amount of *Pediastrum*.
PZ IX (25–0)	0.42–0	Pollen of *Pinus* (up to 45%), *Picea* (20%), *Betula* sect. *Albae* (25%), and *Alnus* (15%) dominate. Presence of *Secale, Triticum, Fagopyrum, Centaurea cyanus, Plantago lanceolata, Artemisia*, Amaranthaceae, *Rumex* and *Cannabis*.

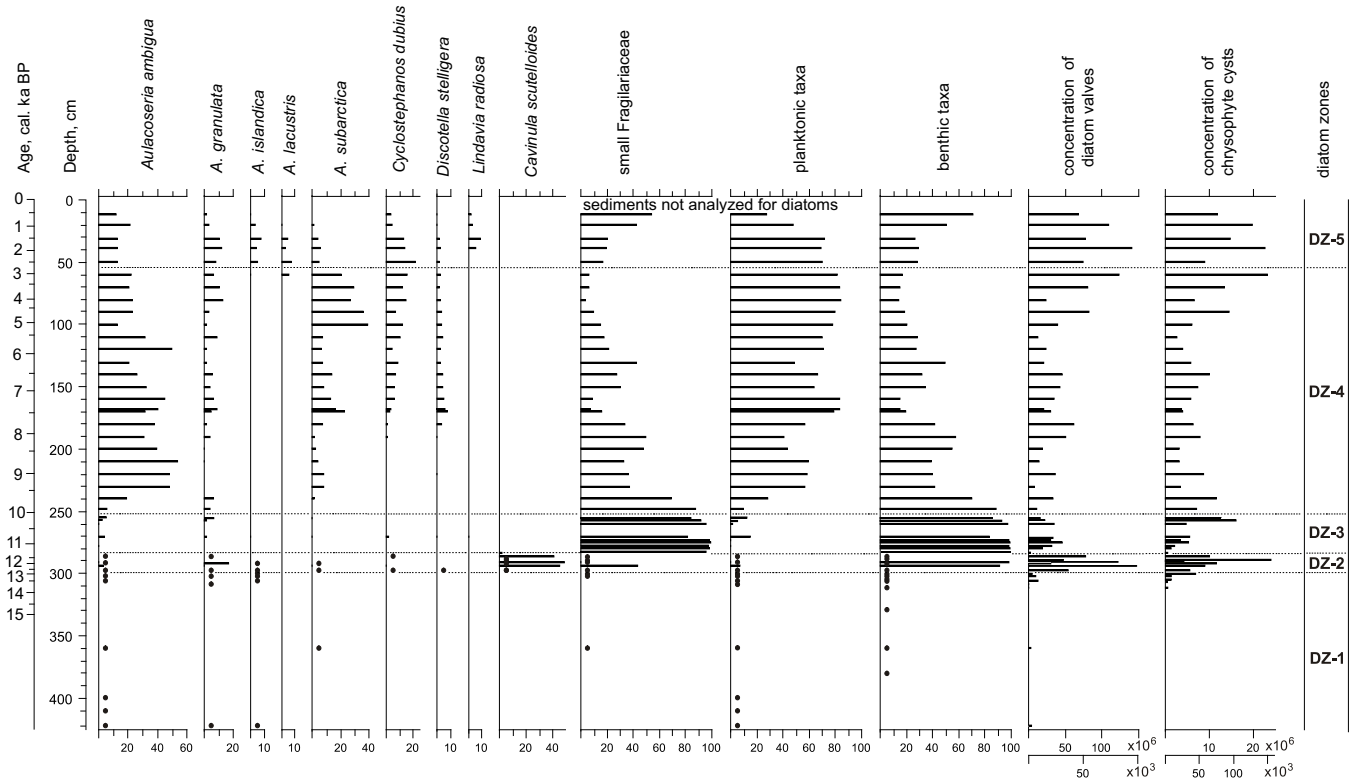

Figure 11. Relative abundances (in percentages) of the main diatom taxa and ecological groups, and concentration of diatom valves and chrysophyte cysts (gray bars, thousands; black bars, millions per 1 g of dry sediment) in Lake Zvan. Black dots indicate presence of taxa in the diatom assemblages where diatom counts were too low to calculate reliable percentages. DZ, diatom zone.

planar-parallel and cross-laminated medium to coarse-grained sands with occasional inclusions of small pebbles) indicate that the initial stages of the lake formation were associated with substantial water and sediment input. The upper part of these deposits (381–315 cm core depth; Fig. 4A), represented by planar-parallel rhythmically laminated clayey silts, reflect sedimentation in a relatively deep cold-water aquatic environment with pronounced differentiation in seasonal conditions. Extremely low concentra-

https://doi.org/10.1017/qua.2025.10020 Published online by Cambridge University Press

Table 5. Main diatom zones (DZ), total organic carbon (TOC), and total nitrogen (TN) content of the Zvan-1 sediment core.

DZ (cm)	Age (cal ka BP)	Dominant diatom assemblages	TOC and TN content
DZ−1 (424–300)	15.5–13.0	Low concentrations of diatom valves (max. 9 × 10^3/g) and chrysophyte cysts (max. 45 × 10^3/g). Sporadic finds of planktonic *Aulacoseira ambigua, Aulacoseira granulata, Aulacoseira islandica*, and small benthic Fragilariaceae.	Extremely low TOC (0.5–0.6%) and TN (0.05–0.1%) between 424 and 340 cm (15.5–13.8 cal ka BP). Rapid increase (up to 7.7% for TOC and 0.8% for TN) upward.
DZ−2 (300–283)	13.0–11.3	Large increase in concentrations of diatoms (to 1.5 × 10^6/g) and chrysophytes (0.29 × 10^6/g) Benthic *Cavinula scutelloides* typical of slightly alkaline shallow waters with sufficient nutrients dominates (≥40%); at some levels planktonic eutrophic *A. ambigua* and small benthic Fragilariaceae, which mainly occur in slightly alkaline environments and a wide range of trophic states are abundant.	TOC and TN contents significantly decrease at 290 cm (ca. 12 cal ka BP).
DZ−3 (283–251)	11.3–9.9	Further increase in diatom and chrysophyte concentrations ≥20 × 10^6/g and 16 × 10^6/g, respectively). Alkaliphilous benthic Fragilariaceae (mainly *Staurosira construens* and *Staurosirella pinnata*, known as pioneer species in initial lake basins and/or in lakes recently isolated from larger lake basins) dominate. Total benthic taxa >80%.	TOC and TN increase upward.
DZ−4 (251–55)	9.9–3.0	Diatom and chrysophyte concentrations further increase, but are highly fluctuating. Planktonic taxa, mostly *Aulacoseira* spp. increase to >80%. Eutrophic alkaliphilous *A. ambigua* dominates (up to 50%). Above 110 cm core depth, the percentage of oligo-mesotrophic *Aulacoseira subarctica* increases to 40%. In the upper DZ−4, abundances of alkaliphilous eutrophic *A. granulata* and alkalibiontic *Cyclostephanos dubius* increase to >10%. Benthic species (mostly *Staurosira construens, Staurosira venter, Staurosirella pinnata*) markedly decrease in the upper DZ−4.	TOC and TN reach their maximum (up to 24.3%, and 2.2%, respectively) between 170 and 100 cm core depths (ca. 7.2–4.5 cal ka BP). The TOC:TN ratio shows a different trend, also increasing gradually, but achieving a maximum (15.8%) above 110 cm core depth (after 4.5 cal ka BP).
DZ−5 (55–11)	3.0–0.5	Diatom and chrysophyte concentrations reach their highest values through the core (>100 × 10^6/g and >20 × 10^6/g, respectively). Planktonic taxa predominate in the lower DZ−5, with the most abundant being *A. ambigua* (up to 23%), *C. dubius* (22%), *A. granulata* (12%), and *A. subarctica* (6%). Neutrophilous *A. islandica* (thriving under a wide range of trophic conditions), acidophilus oligo-mesotrophic *Aulacoseira lacustris*, and alkaliphilous oligo-mesotrophic *Lindavia radiosa* are also present. The proportion of benthic Fragilariaceae (mostly *S. pinnata*) and other benthic taxa increases to 72% in the upper DZ−5.	The TOC:TN ratio remains high until 20 cm core depth (ca. 1 cal ka BP).

tions of diatoms and chrysophyte cysts (Fig. 11) in the Unit IV sediments suggest unfavorable conditions in the aquatic ecosystem resulting in their low productivity. Another important factor influencing microfossil concentrations is the sedimentation rate, as high amounts of mineral particles coming from the catchment cause low diatom concentrations. Such conditions are typical for proglacial lakes or lakes in areas with large volumes of dead ice. However, we can exclude sedimentation in a proglacial lake in front of the ice sheet, as the formation of the GPR Unit IV continued until the Allerød warming (approximately 14 cal ka BP), when the ice margin is reconstructed as being much farther to the north-northwest (Hughes et al., 2016; Gorlach et al., 2017; Gromig et al., 2019). Thus, we can conclude that a relatively large and deep lake dammed by dead ice masses existed in the area of the modern Lake Zvan since the ice retreated (probably already by 17 cal ka BP or even earlier) until approximately 14 cal ka BP. Deposits accumulated in the lake depression during this time were heavily deformed (Fig. 3) shortly after 14 cal ka BP due to thermokarst processes caused by the degradation of the dead ice masses.

The deep-water sediments that accumulated during the Older Dryas (Figs. 4 and 9) are overlain directly by shallow-water deposits dated to 14 cal ka BP. This fact excludes a substantial hiatus in the sediment succession and suggests that melting of the dead ice only occurred in the short time period at the very beginning of the Allerød warming. The radargrams obtained from Lake Piros (Fig. 5) display very similar features in the architecture of the older deformed and younger undeformed deposits. Therefore, the melting of dead ice recognized and dated in the Lake Zvan sediments was not a local event.

We can state that at approximately 14 cal ka BP, the climatic conditions in the Valdai Highlands became favorable for the very rapid degradation of the surviving dead ice masses, which led to the drainage of the ice-dammed lakes system, the release of a huge freshwater volume, and radical changes in the surrounding landscapes. These processes could have led to the reactivation of the

https://doi.org/10.1017/qua.2025.10020 Published online by Cambridge University Press

karst processes in the Valdai Highlands due to the large amounts of meltwater causing aggressive dissolution of carbonate rocks.

Deformations of the GPR Unit IV deposits in Lake Zvan (Figs. 2 and 3) and the analogous sediments in Lake Piros (Fig. 5) can easily be explained by the degradation of dead ice. However, the sagging deformations (Fig. 3) observed in the younger sediments upward to the Late Holocene cannot be explained by the degradation of dead ice during the late glacial. Such deformations in the younger sediments suggest that karst processes played an important role in the formation of the modern lake basin. There are a number of lines of evidence for the substantial shallowing and partial drying out of the lake basin during the subsequent stage. The active erosional processes are evidenced by the truncation at the top of the GPR Unit IV in Lake Zvan (Figs. 2–4) and analogous deposits of Lake Piros (Figs. 5 and 6). A horizon associated with wave erosion is observed in core Zvan-1 (Fig. 4A). The sedimentary structure reflects the sharp changes in the deposition settings as well.

In core Zvan-1 (Fig. 4A), the sediments that accumulated during the Allerød, Younger Dryas, and partly during the Early Holocene are represented by a ca. 50-cm-thick massive silt with a high content of organic debris without any evidence of possible hiatuses. This layer suggests extremely low sedimentation rates in shallow waters and accumulation of reworked organic debris. In core Zvan-2, deposits of this age are represented by peat (Figs. 3 and 4B), again indicating a shallow-water environment, alongside active eutrophic processes in the lake basin. The high content of green algae remains (mostly *Pediastrum*) in these sediments (Fig. 9), as well as in the Allerød sediments in the Piros-1 core (Fig. 10), also reflect shallow-water habitats in both lakes.

The massive silt with a high content of organic debris in the Zvan-1 core (Fig. 4A) corresponds to the diatom zones DZ-2 and DZ-3 (Fig. 11). The increase in the concentration of siliceous microfossils (DZ-2) indicates a change in sedimentation conditions, in particular, a substantial reduction in the amount of allochthonous mineral particles coming into the lake basin, resulting in more favorable conditions for the aquatic biota (particularly diatoms and chrysophytes). The overwhelming dominance of the benthic diatom *Cavinula scutelloides* clearly indicates the shallowing of the lake, with a shift in the environment to more alkaline conditions and increased concentrations of essential nutrients.

A further increase in the productivity of the ecosystem resulted in increased abundances of both groups of siliceous microfossils to several tens of millions (DZ-3). The dominance of benthic *Staurosira construens, Staurosira venter*, and *Staurosirella pinnata* often marks transitional conditions with a dynamic and unstable environment. However, their predominance in DZ-3 (Fig. 11) might also indicate shallow depths, as well as accessibility of substrate for colonization, in particular, macrophytes. These species have been observed among the dominating taxa in Lake Valdai since the Younger Dryas (Davydova et al., 1992, 2001).

The Lake Zvan sediment record reveals the dead ice degradation and drainage of the initial large and deep lake at the beginning of the Allerød. These processes were accompanied by extremely slow sedimentation in the shallow-water environments (Figs. 3B and 4A), peat formation in the swampy areas (Figs. 3C and 4B), and partial erosion of the late glacial sediments (Figs. 3D and 4C) during the end of the late glacial to the Early Holocene. Organic-rich gyttja started to accumulate in the lake after ca. 10 cal ka BP (Fig. 4A), reflecting lake-level rise and the formation of the lake basin similar to the modern one.

Unlike Lake Zvan, two large lakes (Piros and Valdai) show completely different dynamics of lake level during the Early Holocene. In core Piros-1 from Lake Piros, we observe a hiatus between ca. 10.3 and 7.0 cal ka BP (Fig. 6). This hiatus coincides with a hiatus revealed in the Lake Valdai sediment sequence between ca. 10.5 and 8.0 cal ka BP (Davydova et al., 1992, 2001). This low lake-level stand and/or hiatus is not evident in the Early Holocene sediments of smaller lakes located in the same area (Fig. 1), such as Lake Zvan (this study) and Lake Terebenskoye (Wohlfarth et al., 2007; Subetto, 2009). Taking into consideration that small lakes, normally, respond more quickly and more explicitly to temperature and water supply changes, we suggest that the long-lasting low lake-level stand in Lake Piros and Lake Valdai is not directly related to climate conditions. Instead, karst processes resulting in lake drainage could be one possible explanation for the lake level lowering.

In the Zvan-1 core, the onset of consolidated gyttja accumulation occurred shortly after ca. 10.12 cal ka BP (Fig. 4A). This correlates well with previous studies in northwestern Russia (e.g., Wohlfarth et al., 2007; Subetto, 2009). Accumulation of unconsolidated organic sediments (gyttja) is indicative of bioproductivity increase as well as lake-level rise, because gyttja is not formed in very shallow waters.

The composition of the diatom assemblages accumulated between ca. 9.9 and 3.0 cal ka BP (DZ-4 of Fig. 11) suggests relatively warm climate conditions, resulting in the increase of the trophic state of Lake Svan, with a deeper aquatic environment indicated by the dominance of planktonic eutrophic species. Changes in the diatom assemblages in the upper part of DZ-4 (Fig. 11) reflect a trend toward the dominance of planktonic taxa, which might be a result of the increasing water level. The gradually increasing content of *Sphagnum* spores in the upper pollen zones (Fig. 9) starting after 5 cal ka BP most likely reflects paludification in the surrounding areas due to the gradual increase in lake level. This inference is supported by the absence of *Pediastrum* remains in the upper part of PZ VIII (Fig. 9), as this green alga prefers relatively shallow water, and its disappearance from the lake sediments between ca. 5 and 3 cal ka BP points to a deeper lake level during this interval.

The general increase of planktonic diatoms up-core most likely reflects an increasing lake level. The dominance of oligo-mesotrophic *Aulacoseira subarctica* in the upper part of DZ-4 (Fig. 11) indicates a slight decrease in the trophic state of the lake. This is also reflected by changes in the C:N ratio, which reaches its maximum in this interval (Fig. 7), indicating a reduction in autochthonous organic matter.

Diatom assemblages of the uppermost diatom zone of the Zvan-1 core (DZ-5 of Fig. 11) accumulated during the last 3 cal ka BP and reflect possible changes in lake level and trophic state. Higher proportions of planktonic taxa (*Aulacoseira ambigua, Aulacoseira granulata, Cyclostephanos dubius*) in the sediments accumulated between 3 and 1.4 cal ka BP indicate a higher trophic state of the lake and, apparently, a deep-water environment, as the dominance of these taxa points to higher contents of nutrients, especially biogenic silica. The substantial increase in diatom concentration also indicates an increase in lake bioproductivity. Decreasing amounts of benthic diatoms suggest a lower substrate availability for diatom colonization as the lake level rose. Water transparency could also decrease because of excessive phytoplankton growth.

The diatom assemblages from the sediments accumulated after 1.4 cal ka BP (the uppermost 30 cm of DZ-5; Fig. 11) demonstrate a decrease in the ratio of planktonic to benthic diatoms. These changes may indicate the lowering of the lake level due

https://doi.org/10.1017/qua.2025.10020 Published online by Cambridge University Press

to infilling of the lake. These changes to lake status are probably interconnected with the intensification of agricultural land use as revealed in the uppermost pollen zones (PZ IX and X of Fig. 9). This also coincides with the large increase in *Sphagnum* spores, reflecting paludification processes, which could also be connected with human activity in the lake catchment.

Conclusions

The multiproxy studies of sediment cores collected from two lakes in the eastern part of the Valdai Highlands provide a reliable basis for reconstructions of the climate, landscape, and lacustrine system dynamics after ca. 17 cal ka BP. The relatively small hydrologic and ecological systems of the studied lakes are quite sensitive to the regional climate and environmental changes as well as to local human activity.

After the ice sheet retreated from the area after ca. 17 cal ka BP and before the beginning of Allerød warming (~14 cal ka BP), the Valdai Highlands were dominated by dead ice and ice-dammed cold, deep lakes. Abrupt environmental changes occurred shortly after 14 cal ka BP. Most of the dead ice in the Valdai Highlands melted, causing the drainage of the huge ice-dammed lakes and the release of vast landmasses. The appearance of spruce in the local forests at this time marks substantial changes in the vegetation cover and climate conditions. This period can also possibly be associated with reactivation of karst processes in the Valdai Highlands. In the Early Holocene, around 10 cal ka BP, the establishment of the modern types of landscape and lake systems took place in the Valdai Highlands, which is consistent with the onset of organic gyttja sedimentation.

The last ~2500 years in the Valdai Highlands have been characterized by the onset of agricultural land use; a simultaneous drop in temperature; and interconnected environmental consequences such as lake eutrophication, paludification of the catchment areas, and weakening of karst processes.

Acknowledgments. Part of the fieldwork was carried out with the use of the GPR instrument provided by the St. Petersburg State University Center for Geo-Environmental Research and Modeling (GEOMODEL). Research of AL contributes to the State Research Program of the Institute of Limnology, RAS–SPC RAS. The authors are grateful to the Centre of Accelerator Mass Spectrometry at the University of Cologne and personally to Janet Rethemeyer for the dating of lake sediments. The authors are also very grateful to Lewis Owen, Peter Langdon, and two anonymous reviewers for their valuable suggestions, recommendations, and edits, which helped to improve the initial manuscript. Special thanks to Cathy Jenks for English proofreading the final version of the manuscript.

Funding. The fieldwork was funded by the Russian Foundation for Basic Research (RFBR grant 15-05-02584). The work of GF supported by the Republic of Armenia Ministry of Education, Science, Culture and Sports (project–23IRF-1E02).

References

Arslanov, K.A., 1993. Late Pleistocene geochronology of European Russia. *Radiocarbon* **35**, 421–427.

Arslanov, K.A., Savelieva, L.A., Gey, N.A., Klimanov, V.A., Chernov, S.B., Chernova, G.M., Kuzmin, G.F., *et al*. 1999. Chronology of vegetation and paleoclimatic stages of north-western Russia during the Late Glacial and Holocene. *Radiocarbon* **41**, 22–45.

Arslanov, K.A., Savelieva, L.A., Klimanov, V.A., Chernov, S.B., Maksimov, F.E., Tertychnaya, T.V., Subetto, D.A., 2001. New data on chronology of landscape-paleoclimatic stages in northwestern Russia during the Late Glacial and Holocene. *Radiocarbon* **43**, 545–558.

Blaauw, M., Christen, J.A., 2011. Flexible paleoclimate age-depth models using an autoregressive gamma process. *Bayesian Analysis* **6**, 457–474.

Blaauw, M., Christen, J.A., Vazquez, J.E., Belding, T., Theiler, J., Gough, B., Karney, C., 2020. Package 'rbacon'—Age-Depth Modelling Using Bayesian Statistics. Queen's University, Belfast.

Bushtuev, A.G., Koltukova, I.V., Ostrometskaya, E.D., 1971. An Explanatory Note on Geological and Hydrogeological Maps of the USSR of a Scale of 1:200 000. Tikhvin-Onega's Series. Sheet O-36-XVI. [In Russian.] Cartographic Factory of the All-Soviet Union Geological Fund, Moscow.

Cwynar, L.C., Burden, E., McAndrews, J.H., 1979. An inexpensive sieving method for concentrating pollen and spores from fine-grained sediments. *Canadian Journal of Earth Sciences* **16**, 1115–1120.

Dam, H. van, Mertens, A., Sinkeldam, J., 1994. A coded checklist and ecological indicator values of freshwater diatoms from the Netherlands. *Netherlands Journal of Aquatic Ecology* **28**, 117–133.

Davydova, N.N., 1985. *Diatoms as Indicators of the Environmental Conditions of Water-Bodies in the Holocene*. [In Russian.] Nauka, Leningrad.

Davydova, N.N., Kabailene, M.V., Raukas, A.V., Yakushko, O.F. (Eds.), 1992. *History of Lakes to the North of the East-European Plain. The Karelian Isthmus*. [In Russian.] Nauka, St. Petersburg.

Davydova, N.N., Subetto, D.A., Khomutova, V.I., Sapelko, T.V., 2001. Paleolimnology of three lakes in NW Russia. *Journal of Paleolimnology* **26**, 37–51.

Demidov, I.N., Houmark-Nielsen, M., Kjær, K.H., Larsen, E., 2006. The last Scandinavian Ice Sheet in northwestern Russia: ice flow patterns and decay dynamics. *Boreas* **3**, 425–443.

Giesecke, T., Bennett, K.D., 2004. The Holocene spread of *Picea abies* (L.) Karst in Fennoscandia and adjacent areas. *Journal of Biogeography* **31**, 1523–1548.

Gorlach, A., Hang, T., Kalm, V., 2017. GIS-based reconstruction of Late Weichselian proglacial lakes in northwestern Russia and Belarus. *Boreas* **46**, 48–502.

Grichuk, V.P., Zaklinskaya, E.D., 1948. *Analysis of Fossil Pollen and Spores and Its Application in Paleogeography*. [In Russian.] Geografgiz Press, Moscow.

Grimm, E.C. 2004. *TGView*. Illinois State Museum, Research and Collections Center, Springfield.

Gromig, R., Wagner, B., Wennrich, V., Fedorov, G., Savelieva, L., Lebas, E., Krastel, S., *et al*. 2019. Deglaciation history of Lake Ladoga (northwestern Russia) based on varved sediments. *Boreas* **48**, 330–348.

Guiry, M.D., Guiry, G.M., 2024. AlgaeBase (accessed May 17, 2024). National University of Ireland, Galway. http://www.algaebase.org.

Hughes, A.L.C., Gyllencreutz, R., Lohne, Ø.S., Mangerud, J., Svendsen, J.-I., 2016. The last Eurasian ice sheets—a chronological database and time-slice reconstruction, DATED-1. *Boreas* **45**, 1–45.

Juggins, S., 2007. *C2 Version 1.5 User Guide. Software for Ecological and Palaeoecological Data Analysis and Visualisation*. University of Newcastle, Newcastle upon Tyne.

Kalm, V., Gorlach, A., 2014. Impact of bedrock surface topography on spatial distribution of Quaternary sediments and on the flow pattern of late Weichselian glaciers on the East European Craton (Russian Plain). *Geomorphology* **207**, 1–9.

Khotinsky, N.A., 1987. Radiocarbon chronology and correlation of natural and anthropogenic boundaries of the Holocene. In: Petrov O.M. (Ed.), *New Data in Quaternary Geochronology*. [In Russian.] Nauka, Moscow, pp. 39–45.

Khotinsky, N.A., Klimanov, V.A., 1997. Allerød, Younger Dryas and early Holocene palaeoenvironmental stratigraphy. *Quaternary International* **41**/42, 67–70.

Krammer, K., Lange-Bertalot, H., 1986. *Bacillariophyceae*. 1 Teil, *Naviculaceae*. In: Ettl H., Gerloff J., Heynig H., Mollenhauer D. (Eds.), *Süsswasserflora von Mitteleuropa*, Band 2/1. Gustav Fisher, Jena.

Krammer, K., Lange-Bertalot, H., 1988. *Bacillariophyceae*. 2 Teil, *Bacillariaceae, Epithemiaceae, Surirellaceae*. In: Ettl H., Gerloff J., Heynig H., Mollenhauer D. (Eds.), *Susswasserflora von Mitteleuropa*, Band 2/2. Gustav Fisher, Jena.

Krammer, K., Lange-Bertalot, H., 1991a. *Bacillariophyceae*. 3 Teil, *Centrales, Fragilariaceae, Eunotiaceae*. In: Ettl H., Gerloff J., Heynig H., Mollenhauer D. (eds.) *Susswasserflora von Mitteleuropa*, Band 2/3. Gustav Fisher, Stuttgart.

https://doi.org/10.1017/qua.2025.10020 Published online by Cambridge University Press

Krammer, K., Lange-Bertalot, H., 1991b. *Bacillariophyceae*. 4. Teil, *Achnanthaceae*. In: Ettl, H., Gärtner, G., Gerloff, J., Heynig, H., Mollenhauer, D. (Eds.), *Sußwasserflora von Mitteleuropa*, Band 2/4. Gustav Fischer, Heidelberg.

Kremenetski, K.V., Borisova, O.K., Zelikson, E.M., 2000. The Late Glacial and Holocene history of vegetation in the Moscow region. *Paleontological Journal* **34**, 67–74.

Krotova-Putintseva, A.Y., Verbitskiy, V.R., 2012. Preglacial geomorphology of the northern Baltic Lowland and the Valdai Hills, north-western Russia. *Bulletin of the Geological Society of Finland* **84**, 58–68.

Kupriyanova, L.A., Alyoshina, L.A., 1978. *Pollen and Spores of Plants from the Flora of European Part of USSR*. [In Russian.] Komarov Botanical Institute of the USSR Academy of Sciences, Leningrad.

Latałowa, M., van der Knaap, W.O., 2006. Late Quaternary expansion of Norway spruce *Picea abies* (L.) Karst in Europe according to pollen data. *Quaternary Science Reviews* **25**, 2780–2805.

Lohne, O.S., Mangerud, J., Birks, H.H., 2013. Precise ^{14}C ages of the Vedde and Saksunarvatn ashes and the Younger Dryas boundaries from western Norway and their comparison with the Greenland Ice Core (GICC05) chronology. *Journal of Quaternary Science* **28**, 490–500.

Mangerud, J., 2021. The discovery of the Younger Dryas, and comments on the current meaning and usage of the term. *Boreas* **50**, 1–5.

McKay, N.P., Emile-Geay, J., Khider, D., 2021. geoChronR—an R package to model, analyze, and visualize age-uncertain data. *Geochronology* **3**, 149–169.

Moore, P.D., Webb, J.A., Collinson, M.E., 1991. *Pollen analysis*. Blackwell Scientific Publications, Oxford, UK.

Musin, A.G., Kirsanov, V.K., 1990. The features of the karst in the northern part of the Valdai Upland. [In Russian.] *Izvestiya Akademii Nauk SSSR, Seriya Geograficheskaya* **6**, 101–108.

Novenko, E.A., Volkova, E.M., Nosova, N.B., Zuganova, I.S., 2009. Late Glacial and Holocene landscape dynamics in the southern taiga zone of East European Plain according to pollen and macrofossil records from the Central Forest State Reserve (Valdai Hills, Russia). *Quaternary International* **207**, 93–103.

Payne, R.J., Malysheva, E., Tsyganov, A., Pampura, T., Novenko, E., Volkova, E., Babeshko, K., *et al*. 2016. A multi-proxy record of Holocene environmental change, peatland development and carbon accumulation from Staroselsky Moch peatland, Russia. *Holocene* **26**, 314–326.

Reimer, P.J., Austin, W.E.N., Bard, E., Bayliss, A., Blackwell, P.G, Ramsey, C.B., Butzin, M., *et al*. 2020. The IntCal20 Northern Hemisphere Radiocarbon Age Calibration Curve (0–55 cal ka BP). *Radiocarbon* **62**, 725–757.

Rethemeyer, J., Fülöp, R.-H., Höfle, S., Wacker, L., Heinze, S., Hajdas, I., Patt, U., *et al*. 2013. Status report on sample preparation facilities for ^{14}C analysis at the new Cologne AMS center. *Nuclear Instruments and Methods in Physics Research B* **294**, 168–172.

Rinterknecht, V., Hang, T., Gorlach, A., Kohv, M., Kalla, K., Kalm, V., Subetto, D., *et al*. 2018. The Last Glacial Maximum extent of the Scandinavian Ice Sheet in the Valday Heights, western Russia: evidence from cosmogenic surface exposure dating using ^{1o}Be. *Quaternary Science Reviews* **200**, 106–113.

Savelieva, L.A., Andreev, A.A., Gromig, R., Subetto, D.A., Fedorov, G.B., Wennrich, V., Wagner, B., *et al.* 2019. Vegetation and climate changes in northwestern Russia during the Lateglacial and Holocene inferred from the Lake Ladoga pollen record. *Boreas* **48**, 349–360.

Subetto, D.A., 2009. *Lake Bottom Sediments: Paleolimnological Reconstructions*. [In Russian.] Publishing House of Herzen State Pedagogical University, St. Petersburg.

Subetto, D.A., Wohlfarth, B., Davydova, N.N., Sapelko, T., Björkman, L., Solovieva, N., Wastegärd, S., *et al*. 2002. Climate and environment on the Karelian Isthmus, northwestern Russia, 13 000-9000 cal. yrs BP. *Boreas* **31**, 1–19.

Tarasov, P.E., Savelieva, L.A., Long, T., Leipe, Ch., 2019. Postglacial vegetation and climate history and traces of early human impact and agriculture in the present-day cool mixed forest zone of European Russia. *Quaternary International* **516**, 21–41.

Verbitskiy, V.R., Verbitskiy, I.V., Vasil'eva, O.V., Savanin, V.V., Kyamyarya, V.V., Mazurkevich, K.N., Krotova-Putintseva, A.E., *et al*. 2012. An Explanatory Note on a Geological Map of the Russian Federation of a Scale of 1:1 000 000 (Third Generation). [In Russian.] Central European Series. Sheets O-35 (Pskov), (N-35), O-36 (St. Petersburg). VSEGEI Cartographic Factory, St. Petersburg.

Wohlfarth, B., Bennike, O., Brunnberg, L., Demidov, I., Possnert, G., Vyahirev, S., 1999. AMS ^{14}C measurements and macrofossil analysis from a varved sequence near Pudozh, eastern Karelia, NW Russia. *Boreas* **29**, 575–586.

Wohlfarth, B., Filimonova, L., Bennike, O., Björkman, L., Brunnberg, L., Lavrova, N., Demidov, I. *et al*. 2002. Late-glacial and early Holocene environmental and climatic change from Lake Tambichozero in southeastern Russian Karelia. *Quaternary Research* **58**, 261–272.

Wohlfarth, B., Lacourse, T., Bennike, O., Subetto, D., Filimonova, L., Tarasov, P., Sapelko, T. *et al*. 2007. Climatic and environmental changes in north-western Russia between 15 000 and 8 000 cal yr BP: a review. *Quaternary Science Reviews* **26**, 1871–1883.

Wohlfarth, B., Schwark, L., Bennike, O., Filimonova, L., Tarasov, P., Björkman, L., Brunnberg, L., *et al*. 2004. Unstable early Holocene climatic and environmental conditions in northwestern Russia derived from a multidisciplinary study of a lake sediment sequence from Pichozero, southeastern Russian Karelia. *Holocene* **14**, 732–746.

Wohlfarth, B., Tarasov, P., Bennike, O., Lacourse, T., Subetto, D.A., Torssander, P., Romanenko, F. 2006. Late glacial and Holocene palaeoenvironmental changes in the Rostov-Yaroslavl' area, West Central Russia. *Journal of Paleolimnology* **35**, 543–569.

https://doi.org/10.1017/qua.2025.10020 Published online by Cambridge University Press